Preprint 02-2009

On the implementation of rate-independent standard dissipative solids at finite strain – Variational constitutive updates

J. Mosler & O.T. Bruhns

This is a preprint of an article accepted by:

Computer Methods in Applied Mechanics and Engineering (2009)

GKSS Research Centre Geesthacht
Materials Mechanics

On the implementation of rate-independent standard dissipative solids at finite strain – Variational constitutive updates

J. Mosler

Materials Mechanics
Institute for Materials Research
GKSS Research Centre
D-21502 Geesthacht, Germany
E-Mail: joern.mosler@gkss.de

O.T. Bruhns

Institute of Mechanics
Ruhr University Bochum
Ruhr University Bochum
D-44780 Bochum, Germany
E-Mail: bruhns@tm.bi.rub.de

SUMMARY

This paper is concerned with an efficient, variationally consistent, implementation for rate-independent dissipative solids at finite strain. More precisely, focus is on finite strain plasticity theory based on a multiplicative decomposition of the deformation gradient. Adopting the formalism of standard dissipative solids which allows to describe constitutive models by means of only two potentials being the Helmholtz energy and the yield function (or equivalently, a dissipation functional), finite strain plasticity is recast into an equivalent minimization problem. In contrast to previous models, the presented framework covers isotropic and kinematic hardening as well as isotropic and anisotropic elasticity and yield functions. Based on this approach a novel numerical implementation representing the main contribution of the paper is given. In sharp contrast to by now classical approaches such as the return-mapping algorithm and analogously to the theoretical part, the numerical formulation is variationally consistent, i.e., all unknown variables follow naturally from minimizing the energy of the considered system. Consequently, several different numerically efficient and robust optimization schemes can be directly employed for solving the resulting minimization problem. Extending previously published works on variational constitutive updates, the advocated model does not rely on any material symmetry and therefore, it can be applied to a broad range of different plasticity theories. As two examples, an anisotropic Hill-type and a Barlat-type model are implemented. Numerical examples demonstrate the applicability and the performance of the proposed implementation.

1 Introduction

Nowadays, computational plasticity represents an indispensable tool for the design of complex engineering structures. Considering a certain time interval $[t_n; t_{n+1}]$, the goal of computational plasticity is the calculation of all state and history variables $\boldsymbol{X}$ at time t_{n+1}, i.e., $\boldsymbol{X}_n \rightarrow \boldsymbol{X}_{n+1}$. Such methods are usually based on a time integration transforming the underlying differential equations such as the evolution laws into a set of non-linear equations. Subsequently, the resulting algebraic problem is solved iteratively. A typical example is given by the return-mapping algorithm, cf. [1, 2]. This well-established first-order scheme consists of an (implicit) backward-Euler integration combined with a Newton-iteration. By now, the return-mapping algorithm can be considered as a state-of-the-art method even for the geometrically exact framework (large strains), cf. [3–10]. Most frequently, the underlying mechanical models are based

on a multiplicative decomposition of the deformation gradient ($\boldsymbol{F} = \boldsymbol{F}^{\mathrm{e}} \cdot \boldsymbol{F}^{\mathrm{p}}$). Although many fundamental problems in finite strain elastoplasticity are still unanswered (see, e.g. [11, 12]), the kinematical assumption $\boldsymbol{F} = \boldsymbol{F}^{\mathrm{e}} \cdot \boldsymbol{F}^{\mathrm{p}}$ is also made in the present work.

Mathematically, plasticity theory represents a non-smooth and highly non-linear problem in general. Clearly, the non-smoothness is a direct consequence of the elastic-plastic transition, while non-linearity results from the evolution equations, cf. [1, 2]. Even worse, many plasticity models lead to non-unique solutions. For instance, crystal plasticity theory in the sense of Schmid shows this problem (see [13]). Due to these aforementioned issues, computational plasticity, although already established in the 60s (see [14]), is far from being completely solved and the development of an efficient and robust numerical implementation is not straightforward at all, cf. [15].

If the evolution equations and the flow rule obey the so-called normality rule (associative models), they can be elegantly derived from a variational principle – the postulate of maximum dissipation, cf. [16]. Comi and co-workers realized that by recourse to time discretization, a similar variational concept can be derived even for the discrete setting, see [17, 18]. In those works, the authors, derived a Hu-Washizu functional whose minimum corresponds to the solution of the discretized algebraic differential equations defining the material model. In the respective numerical implementation, the constitutive model was enforced in a weak sense. That is, the resulting finite element formulation is different compared to the one usually applied in computational plasticity, cf. [1, 2], i.e., a pointwise description (usually at the integration points).

Probably inspired by the works [17, 18], Ortiz and co-workers advocated a constitutive update based on a minimization principle as well, cf. [19–21]. Nevertheless, in contrast to the previous works, the proposed algorithmic formulation coincides with the structure of standard finite element codes. More precisely, the update is performed pointwise at the integration points. Similar numerical procedure and further elaborations can be found, for instance, in [22–28]. For models based on linearized kinematics, the reader is referred to [29].

The advantages resulting from such a variational constitutive update are manifold. On the one hand, the existence of solutions can be analyzed by using the same tools originally designed for hyperelastic material models, cf. [21, 22, 30]. On the other hand, a minimum principle can be taken as a canonical basis for error estimation, cf. [20, 31–33]. Additionally, from an implementational point of view, a minimization principle opens up the possibility to apply state of the art optimization algorithms. Particularly for multisurface plasticity models such as single-crystal plasticity this represents an interesting feature, cf. [19].
It is noteworthy that if a backward-Euler integration, together with a Newton scheme, is employed for solving the aforementioned minimization problem, variational updates are equivalent to the return-mapping algorithm in many cases, see [33]. Obviously, this implies that variational constitutive updates are a priori more efficient than the return-mapping scheme, since other, better suited, optimization strategies can be applied as well.

In the present paper, an enhanced constitutive update for so-called standard dissipative solids obeying the postulate of maximum dissipation, in line with [19, 20, 22–25, 28, 29], is elaborated. In contrast to the algorithms discussed in the cited works, the advocated novel scheme does not rely on any material symmetry and therefore, it can be applied to a broad range of different plasticity theories. More precisely, arbitrary material symmetries concerning the elastic response and the yield function can be taken into account. Furthermore, kinematic and coupled isotropic/kinematic hardening are covered by the novel algorithmic formulation. It is noteworthy that the new advocated implementation includes, as a special case, the model proposed in [28]. Within the cited recent paper, an algorithmic, variationally consistent, formulation for a class of von Mises models is given. Extending the aforementioned paper significantly, two

prototype implementations, a fully anisotropic Hill-type and an orthotropic Barlat-type model [34], are implemented.

The paper is organized as follows: Section 2 is concerned with a concise review of finite strain plasticity theory based on a multiplicative decomposition of the deformation gradient ($\boldsymbol{F} = \boldsymbol{F}^{\mathrm{e}} \cdot \boldsymbol{F}^{\mathrm{p}}$). While Subsection 2.1 covers the fundamentals, the variational structure of plasticity associated with so-called standard dissipative solids is discussed in Subsection 2.2. Section 2 is completed by a relatively complex example: a fully anisotropic broad family of plasticity models characterized by yield functions being positively homogeneous of degree n (Subsection 2.3). The main contribution of the present paper dealing with a novel numerical implementation suitable for standard dissipative solids at finite strain is addressed in Section 3. The underlying key idea is to conveniently parameterize the restrictions imposed by the flow and the hardening rules. Finally, the performance and the robustness of the resulting algorithmic formulation are demonstrated by means of selected numerical examples (Section 4).

2 Finite strain plasticity theory

The fundamentals of a variationally consistent finite strain plasticity theory based on a multiplicative decomposition of the deformation gradient in the sense of [35] are briefly discussed in this section. For the sake of simplicity, isothermal static conditions are assumed. For modeling a dissipative material response, a description with internal state variables is used, cf. [36]. While Subsection 2.1 is concerned with a concise review of conventional plasticity theory at finite strains, standard dissipative solids are addressed in Subsection 2.2. These models allow to describe plasticity theories by means of only two independent functionals being the Helmholtz energy and the yield function (or equivalently, a dissipation functional). The present section is completed a complex example: a variationally consistent, fully anisotropic broad family of plasticity models characterized by yield functions being positively homogeneous of degree n (Subsection 2.3).

2.1 Fundamentals

Without going too much into detail and following Lee [35], a multiplicative decomposition of the deformation gradient $\boldsymbol{F} := \mathrm{GRAD}\boldsymbol{\varphi}$ into an elastic part $\boldsymbol{F}^{\mathrm{e}}$ and a plastic part $\boldsymbol{F}^{\mathrm{p}}$ of the type

$$\boldsymbol{F} = \boldsymbol{F}^{\mathrm{e}} \cdot \boldsymbol{F}^{\mathrm{p}}, \qquad \text{with} \qquad \det \boldsymbol{F}^{\mathrm{e}} > 0,\ \det \boldsymbol{F}^{\mathrm{p}} > 0 \tag{1}$$

is adopted. For a comprehensive overview and critical comments on different plasticity formulations at finite strains, refer to [12, 37, 38]. Based on the split (1), the Helmholtz energy of the considered solid can be written as

$$\Psi = \Psi(\boldsymbol{F}^{\mathrm{e}}, \boldsymbol{F}^{\mathrm{p}}, \boldsymbol{\alpha}) \tag{2}$$

see [1, 2, 39, 40]. Here, $\boldsymbol{\alpha} \in \mathbb{R}^n$ is a collection of strain-like internal variables associated with hardening or softening. Assuming that the elastic response modeled by $\bar{\Psi}^{\mathrm{e}}$ is completely independent of the internal processes reproduced by $\boldsymbol{\alpha}$, an energy functional Ψ of the type

$$\Psi = \bar{\Psi}^{\mathrm{e}}(\boldsymbol{F}^{\mathrm{e}}) + \Psi^{\mathrm{p}}(\boldsymbol{\alpha}) \tag{3}$$

is adopted. Clearly, by the principle of material frame indifference, $\bar{\Psi}^{\mathrm{e}}(\boldsymbol{F}^{\mathrm{e}}) = \Psi^{\mathrm{e}}(\boldsymbol{C}^{\mathrm{e}})$ where $\boldsymbol{C}^{\mathrm{e}} := \boldsymbol{F}^{\mathrm{e}^T} \cdot \boldsymbol{F}^{\mathrm{e}}$ is the elastic right Cauchy-Green tensor. The second term in Eq. (3), denoted as Ψ^{p}, represents the stored energy due to plastic work. It is associated with isotropic/kinematic

hardening/softening. For more details about energy functionals of the type (3), refer to [41]. It should be noted that in most applications, a functional of the type (3) is chosen.

Considering an isothermal process, the second law of thermodynamics yields

$$\mathcal{D} = \boldsymbol{P} : \dot{\boldsymbol{F}} - \dot{\Psi} = \boldsymbol{S} : \frac{1}{2}\,\dot{\boldsymbol{C}} - \dot{\Psi} \geq 0 \tag{4}$$

and finally, by using Eq. (1) and (3) the dissipation $\mathcal{D}$ reads

$$\mathcal{D} = \left(\boldsymbol{F}^{\mathrm{p}} \cdot \boldsymbol{S} \cdot \boldsymbol{F}^{p^T} - 2\,\frac{\partial \Psi}{\partial \boldsymbol{C}^{\mathrm{e}}} \right) : \frac{1}{2}\,\dot{\boldsymbol{C}}^{\mathrm{e}} + \boldsymbol{S} : \left(\boldsymbol{F}^{\mathrm{p}^T} \cdot \boldsymbol{C}^{\mathrm{e}} \cdot \dot{\boldsymbol{F}}^{\mathrm{p}} \right) + \boldsymbol{Q} \cdot \dot{\boldsymbol{\alpha}} \geq 0. \tag{5}$$

In Eqs. (4) and (5), $\boldsymbol{P}$ and $\boldsymbol{S} := \boldsymbol{F}^{-1} \cdot \boldsymbol{P}$ denote the first and the second Piola-Kirchhoff stress tensor and $\boldsymbol{Q} := -\partial_{\boldsymbol{\alpha}} \Psi$ is the stress-like internal variable work conjugate to $\boldsymbol{\alpha}$. According to Ineq. (5), the dissipation is decomposed additively into one part associated with the elastic strain rate and a second part corresponding to plastic deformation. Since both parts are independent of one another, Ineq. (5) gives rise to

$$\boldsymbol{S} = 2\,\frac{\partial \Psi}{\partial \boldsymbol{C}} = 2\,\boldsymbol{F}^{\mathrm{p}^{-1}} \cdot \frac{\partial \Psi}{\partial \boldsymbol{C}^{\mathrm{e}}} \cdot \boldsymbol{F}^{\mathrm{p}^{-T}} \tag{6}$$

and the reduced dissipation inequality

$$\mathcal{D} = \boldsymbol{\Sigma} : \boldsymbol{L}^{\mathrm{p}} + \boldsymbol{Q} \cdot \dot{\boldsymbol{\alpha}} \geq 0. \tag{7}$$

Here and henceforth, $\boldsymbol{\Sigma} = 2\,\boldsymbol{C}^{\mathrm{e}} \cdot \partial_{\boldsymbol{C}^{\mathrm{e}}} \Psi$ are the Mandel stresses (cf. [42]) and $\boldsymbol{L}^{\mathrm{p}} = \dot{\boldsymbol{F}}^{\mathrm{p}} \cdot \boldsymbol{F}^{\mathrm{p}^{-1}}$ denotes the plastic velocity gradient. It bears emphasis that both objects belong to the intermediate configuration. This is sometimes highlighted by using overlined letters.

Next, the elastic domain has to be defined. For that purpose, an admissible stress space $\mathbb{E}_{\boldsymbol{\sigma}}$ is introduced, cf. [39]. Here, $\mathbb{E}_{\boldsymbol{\sigma}}$ is formulated in terms of $\boldsymbol{\Sigma}$, i. e.,

$$\mathbb{E}_{\boldsymbol{\sigma}} = \left\{ (\boldsymbol{\Sigma}, \boldsymbol{Q}) \in \mathbb{R}^{9+n} \;\middle|\; \phi(\boldsymbol{\Sigma}, \boldsymbol{Q}) \leq 0 \right\}. \tag{8}$$

Clearly, other stresses such as Cauchy stresses could be utilized as well. The boundary $\partial \mathbb{E}_{\boldsymbol{\sigma}}$ represents a level set function measuring the elastic limit of the considered material. That is, if $(\boldsymbol{\Sigma}, \boldsymbol{Q}) \in \mathrm{int}\mathbb{E}_{\boldsymbol{\sigma}}$, the solid deforms purely elastically. Only if $(\boldsymbol{\Sigma}, \boldsymbol{Q}) \in \partial \mathbb{E}_{\boldsymbol{\sigma}}$, a plastic response is possible. Clearly, the *yield function* ϕ has to be derived from experimental observation. Additionally, ϕ must be convex and sufficiently smooth, cf. [43]. The constitutive model is completed by evolution equations for $\boldsymbol{L}^{\mathrm{p}}$ and $\boldsymbol{\alpha}$ and by loading/unloading conditions. They can be naturally derived from the postulate of maximum dissipation. More precisely,

$$\max_{(\tilde{\boldsymbol{\Sigma}}, \tilde{\boldsymbol{Q}}) \in \mathbb{E}_{\boldsymbol{\sigma}}} \left[\tilde{\boldsymbol{\Sigma}} : \boldsymbol{L}^{\mathrm{p}} + \tilde{\boldsymbol{Q}} \cdot \dot{\boldsymbol{\alpha}}] \right]. \tag{9}$$

This postulate leads to the evolution equations

$$\boldsymbol{L}^{\mathrm{p}} = \lambda\, \partial_{\boldsymbol{\Sigma}} \phi \qquad \dot{\boldsymbol{\alpha}} = \lambda\, \partial_{\boldsymbol{Q}} \phi, \tag{10}$$

together with the Karush-Kuhn-Tucker conditions

$$\lambda \geq 0 \qquad \phi\, \lambda \geq 0. \tag{11}$$

As a result, plastic deformations require $(\boldsymbol{\Sigma}, \boldsymbol{Q}) \in \partial \mathbb{E}_{\boldsymbol{\sigma}}$. The plastic multiplier λ is obtained from the consistency condition

$$\dot{\phi} = 0. \tag{12}$$

Evolution laws of the type (10) are characterized by the property that the rates of the internal variables (together with $\boldsymbol{L}^{\mathrm{p}}$) are proportional to the gradient of the yield function. Clearly, such laws are referred to as *associated flow rules* or *normality rules*.

2.2 Standard dissipative solids

In this section, the plasticity framework discussed before is recast into an equivalent minimization problem. More precisely, the goal of this section is the derivation of a potential, from which the unknown deformation mapping can be computed by minimization. Evidently, for path-dependent problems such as plasticity theory, this potential is defined pointwise (with respect to the (pseudo) time). As in the previous sections, isothermal conditions are assumed and dynamical effects are neglected. This section follows to a large extent [19, 22]. However, it should be pointed out that in contrast to conventional plasticity theories, the variational formulation as advocated in [19, 28] is not based on the introduction of a yield function. Instead of that, the flow rule represents the primitive postulate. The yield function depending on this rule follows from the variational update. In this section, and similar to [22], the existence of a yield function is a priori assumed.

In line with [19, 22], the functional

$$\tilde{\mathcal{E}}(\dot{\boldsymbol{\varphi}}, \dot{\boldsymbol{F}}^{\mathrm{p}}, \dot{\boldsymbol{\alpha}}, \boldsymbol{\Sigma}, \boldsymbol{Q}) = \dot{\Psi}(\dot{\boldsymbol{\varphi}}, \dot{\boldsymbol{F}}^{\mathrm{p}}, \dot{\boldsymbol{\alpha}}) + \mathcal{D}(\dot{\boldsymbol{F}}^{\mathrm{p}}, \dot{\boldsymbol{\alpha}}, \boldsymbol{\Sigma}, \boldsymbol{Q}) + J(\boldsymbol{\Sigma}, \boldsymbol{Q}) \tag{13}$$

is introduced. Here, J is the characteristic function of $\mathbb{E}_{\boldsymbol{\sigma}}$, i.e.,

$$J(\boldsymbol{\Sigma}, \boldsymbol{Q}) := \begin{cases} 0 & \forall (\boldsymbol{\Sigma}, \boldsymbol{Q}) \in \mathbb{E}_{\boldsymbol{\sigma}} \\ \infty & \text{otherwise.} \end{cases} \tag{14}$$

As a result, for admissible stress states, i. e., $(\boldsymbol{\Sigma}, \boldsymbol{Q}) \in \mathbb{E}_{\boldsymbol{\sigma}}$, $\tilde{\mathcal{E}}$ represents the sum of the rate of the stored energy and the dissipation. More precisely, if $(\boldsymbol{\Sigma}, \boldsymbol{Q}) \in \mathbb{E}_{\boldsymbol{\sigma}}$,

$$\tilde{\mathcal{E}}(\dot{\boldsymbol{\varphi}}, \dot{\boldsymbol{F}}^{\mathrm{p}}, \dot{\boldsymbol{\alpha}}, \boldsymbol{\Sigma}, \boldsymbol{Q}) = \boldsymbol{P} : \dot{\boldsymbol{F}} =: \mathcal{P}. \tag{15}$$

That is, $\tilde{\mathcal{E}}$ equals the stress power denoted as $\mathcal{P}$. Inadmissible stress states are penalized by $J = \infty$. The interesting properties of the functional (13) become apparent, if the stationarity conditions are computed. A variation of $\tilde{\mathcal{E}}$ with respect to $(\boldsymbol{\Sigma}, \boldsymbol{Q})$ leads to

$$(\boldsymbol{L}^{\mathrm{p}}, \dot{\boldsymbol{\alpha}}) \in \partial J. \tag{16}$$

where ∂J is the sub-differential of J. The respective equation associated with $\dot{\boldsymbol{\alpha}}$ reads

$$\boldsymbol{Q} = -\frac{\partial \Psi}{\partial \boldsymbol{\alpha}}. \tag{17}$$

Finally, a variation with respect to $\dot{\boldsymbol{F}}^{\mathrm{p}}$ yields

$$\boldsymbol{\Sigma} = \boldsymbol{F}^{\mathrm{e}^T} \cdot \frac{\partial \Psi}{\partial \boldsymbol{F}^{\mathrm{e}}} = 2\, \boldsymbol{C}^{\mathrm{e}} \cdot \frac{\partial \Psi}{\partial \boldsymbol{C}^{\mathrm{e}}}. \tag{18}$$

As a consequence, the stationarity condition of $\tilde{\mathcal{E}}$ results in the flow rule (16), the constitutive relation for the internal stress-like variables (17) and the constitutive relation for the Mandel stresses $\boldsymbol{\Sigma}$. The remaining variation of $\tilde{\mathcal{E}}$ with respect to $\dot{\boldsymbol{\varphi}}$ will be discussed later.

According to [19, 22], it is possible to derive a reduced functional, denoted as $\mathcal{E}$, which only depends on the rate of the deformation and the strain-like internal variables $\boldsymbol{\alpha}$ and $\boldsymbol{F}^{\mathrm{p}}$. For that purpose, $\mathcal{E}$ is re-written by applying the Legendre transformation

$$J^*(\bar{\boldsymbol{L}}^{\mathrm{p}}, \dot{\bar{\boldsymbol{\alpha}}}) = \sup \left\{ \boldsymbol{\Sigma} : \bar{\boldsymbol{L}}^{\mathrm{p}} + \boldsymbol{Q} \cdot \dot{\bar{\boldsymbol{\alpha}}} \;\middle|\; (\boldsymbol{\Sigma}, \boldsymbol{Q}) \in \mathbb{E}_{\boldsymbol{\sigma}} \right\} \tag{19}$$

of J, ,i.e., the postulate of maximum dissipation is applied. Since J^* is positively homogeneous of degree one, a maximization of $\tilde{\mathcal{E}}$ with respect to $(\boldsymbol{\Sigma}, \boldsymbol{Q})$, results in

$$\mathcal{E}(\dot{\boldsymbol{\varphi}}, \dot{\boldsymbol{F}}^{\mathrm{p}}, \dot{\boldsymbol{\alpha}}) = \dot{\Psi}(\dot{\boldsymbol{\varphi}}, \dot{\boldsymbol{F}}^{\mathrm{p}}, \dot{\boldsymbol{\alpha}}) + J^*(\dot{\boldsymbol{L}}^{\mathrm{p}}, \dot{\boldsymbol{\alpha}}). \tag{20}$$

Hence, the only remaining variables are $\dot{\boldsymbol{\varphi}}$, $\dot{\boldsymbol{F}}^{\mathrm{p}}$ and $\dot{\boldsymbol{\alpha}}$. Even more importantly, the strain-like internal variables $\boldsymbol{F}^{\mathrm{p}}$ and $\boldsymbol{\alpha}$ follow jointly from the minimization principle

$$\overset{\circ}{\Psi}_{\mathrm{red}}\,(\dot{\boldsymbol{\varphi}}) := \inf_{\dot{\boldsymbol{F}}^{\mathrm{p}}, \dot{\boldsymbol{\alpha}}} \mathcal{E}(\dot{\boldsymbol{\varphi}}, \dot{\boldsymbol{F}}^{\mathrm{p}}, \dot{\boldsymbol{\alpha}}) \tag{21}$$

which, itself, gives rise to the introduction of the reduced functional $\overset{\circ}{\Psi}_{\mathrm{red}}$ depending only on the deformation mapping. It is interesting to note that for hyperelastic continua, $\overset{\circ}{\Psi}_{\mathrm{red}}$ equals the rate of the strain-energy density, i. e.,

$$\overset{\circ}{\Psi}_{\mathrm{red}}\,(\dot{\boldsymbol{\varphi}}) = \dot{\Psi}(\dot{\boldsymbol{\varphi}}). \tag{22}$$

As a result, in this case, $\overset{\circ}{\Psi}_{\mathrm{red}}$ represents the time derivative of a potential. Further elaborating this analogy, it can be shown that the time integration of Eq. (21) or Eq. (22) over the interval $[t_n, t_{n+1}]$ defines an incremental potential which acts like a standard hyperelastic energy functional for the stresses. Hence, the first Piola-Kirchhoff type stresses are obtained from

$$\boldsymbol{P} = \frac{\partial \left(\int_{t_n}^{t_{n+1}} \overset{\circ}{\Psi}_{\mathrm{red}}\,(\dot{\boldsymbol{\varphi}})\,\mathrm{d}t \right)}{\partial \boldsymbol{F}}. \tag{23}$$

It bears emphasis that if $\overset{\circ}{\Psi}_{\mathrm{red}}$ represents the time derivative of a potential, the standard hyperelastic relation is recovered, i.e., $\boldsymbol{P} = \partial_{\boldsymbol{F}} \Psi$. Applying Eq. (23) it is relatively straightforward to extend the principle of minimum potential energy to standard dissipative solids. More precisely, the unknown deformation mapping $\boldsymbol{\varphi}$ follows from the minimization principle

$$\boldsymbol{\varphi} = \arg \inf_{\boldsymbol{\varphi}} I_{\mathrm{inc}}(\boldsymbol{\varphi}). \tag{24}$$

with the incremental potential $I_{\mathrm{inc}}(\boldsymbol{\varphi})$ being defined as

$$I_{\mathrm{inc}}(\boldsymbol{\varphi}) = \inf_{\boldsymbol{F}^{\mathrm{p}}, \boldsymbol{\alpha}} \left[\int_{\Omega} \int_{t_n}^{t_{n+1}} \mathcal{E}(\dot{\boldsymbol{\varphi}}, \dot{\boldsymbol{F}}^{\mathrm{p}}, \dot{\boldsymbol{\alpha}})\,\mathrm{d}t\,\mathrm{d}V - \int_{\Omega} \rho_0\, \boldsymbol{B} \cdot \boldsymbol{\varphi}\,\mathrm{d}V - \int_{\partial_2 \Omega} \bar{\boldsymbol{T}} \cdot \boldsymbol{\varphi}\,\mathrm{d}A \right]. \tag{25}$$

Here, ρ_0, $\boldsymbol{B}$ and $\bar{\boldsymbol{T}}$ denote the referential density, prescribed body forces and prescribed surface forces acting at $\partial_2 \Omega$.

For a more detailed derivation, the interested reader is referred to [19, 22]. It should be pointed out that the minimization path of the internal variables according to Problem (25) can only be computed analytically for selected, relatively simple examples, cf. [22]. Hence, an efficient numerical implementation as proposed in the following section is required in general.

Remark 1. The presented framework is restricted to isothermal, rate-independent plasticity. However, the extensions necessary for rate-dependent effects such as viscoplasticity are straightforward. More precisely, and in line with [19], an additional term depending on the rate of the inelastic strains has simply to be added to Eq. (20) in this case. Details about the non-trivial extensions required for viscoelasticity or thermomechanically coupled problems which are beyond the scope the present paper can be found in [24, 25, 28].

2.3 Prototype models: positively homogeneous yield functions of degree n

For the sake of concreteness, a prototype model falling into the range of the aforementioned standard dissipative solids is given. Since the main contribution of the present paper is the derivation of an efficient implementation which holds for a broad range of constitutive models including elastic and plastic anisotropy and kinematic hardening, a model combining all these physical phenomena is considered. In the case of a fully isotropic von Mises plasticity formulation, single slip systems or crystal plasticity, refer to [19, 22].

The first component of the model is the stored energy functional. In line with Eq. (3), the Helmholtz energy

$$\Psi(\boldsymbol{F}^{\mathrm{e}}, \alpha_{\mathrm{i}}, \boldsymbol{\alpha}_{\mathrm{k}}) := \Psi^{\mathrm{e}}(\boldsymbol{F}^{\mathrm{e}}) + \Psi^{\mathrm{p}}(\alpha_{\mathrm{i}}, \boldsymbol{\alpha}_{\mathrm{k}}) \tag{26}$$

is further decomposed into the part $\Psi^{\mathrm{p}}_{\mathrm{i}}$ associated with isotropic hardening, while $\Psi^{\mathrm{p}}_{\mathrm{k}}$ corresponds to kinematic hardening, i.e.,

$$\Psi^{\mathrm{p}}(\boldsymbol{\alpha}_{\mathrm{k}}) = \Psi^{\mathrm{p}}_{\mathrm{i}}(\alpha_{\mathrm{i}}) + \Psi^{\mathrm{p}}_{\mathrm{k}}(\boldsymbol{\alpha}_{\mathrm{k}}). \tag{27}$$

Here, the internal strain-like variables α_{i} and $\boldsymbol{\alpha}_{\mathrm{k}}$ are scalar-valued and second-order tensors, respectively. It bears emphasis that no assumption concerning the elastic or the plastic isotropy has been made yet. Hence, for instance, by introducing structural tensors into $\Psi^{\mathrm{e}}(\boldsymbol{F}^{\mathrm{e}})$, elastic anisotropy can be taken into account. Furthermore, it is noteworthy that if $\Psi^{\mathrm{p}}_{\mathrm{k}}(\boldsymbol{\alpha}_{\mathrm{k}})$ is isotropic, its material time derivative reads

$$\dot{\Psi}^{\mathrm{p}}_{\mathrm{k}} = \partial_{\boldsymbol{\alpha}_{\mathrm{k}}} \Psi^{\mathrm{p}}_{\mathrm{k}} \cdot \dot{\boldsymbol{\alpha}}_{\mathrm{k}} = \partial_{\boldsymbol{\alpha}_{\mathrm{k}}} \Psi^{\mathrm{p}}_{\mathrm{k}} \cdot \overset{\circ}{\boldsymbol{\alpha}}_{\mathrm{k}} \tag{28}$$

with $\overset{\circ}{\boldsymbol{\alpha}}_{\mathrm{k}}$ being an arbitrary corotational (objective) time derivative, cf. [44]. This property can be useful for deriving objective evolution equations. While the choice of the isotropic response ($\Psi^{\mathrm{p}}_{\mathrm{i}}$) depending on experiments is uncomplicated, the part describing kinematic hardening is far from being trivial. For a detailed discussion about this issue in the context of a geometrically linearized theory, refer to [45]. For the sake of simplicity and even more importantly, for the sake of interpretableness of the numerical results reported in Section 4, linear hardening is considered, i.e.,

$$\Psi^{\mathrm{p}}_{\mathrm{i}}(\alpha_{\mathrm{i}}) = \frac{1}{2}\, H_{\mathrm{i}}\, \alpha_{\mathrm{i}}^2, \qquad \Psi^{\mathrm{p}}_{\mathrm{k}}(\boldsymbol{\alpha}_{\mathrm{k}}) = \frac{1}{2}\, H_{\mathrm{k}}\, ||\boldsymbol{\alpha}_{\mathrm{k}}||^2 \tag{29}$$

However, this assumption is not crucial for the numerical implementation presented in the following section. Thus, the algorithmic formulation covers more complicated hardening models as well. For instance, an exponential isotropic hardening model is applied in Section 4.2.

The next component of the prototype model is the yield function spanning the admissible stress space. For that purpose, it is assumed that the second-order tensor $\boldsymbol{Q}_{\mathrm{k}}$ represents the back-stress, i.e.,

$$\phi(\boldsymbol{\Sigma}, \boldsymbol{Q}_{\mathrm{k}}, Q_{\mathrm{i}}) = \phi(\boldsymbol{\Sigma} - \boldsymbol{Q}_{\mathrm{k}}, Q_{\mathrm{i}}). \tag{30}$$

Clearly, this assumption is not very restrictive and holds for almost all frequently applied plasticity models. The final postulate being made is that the yield function represents a positively homogeneous function of degree n. More precisely,

$$\phi(\boldsymbol{\Sigma}, \boldsymbol{Q}_{\mathrm{k}}, Q_{\mathrm{i}}) = \Sigma^{\mathrm{eq}}(\boldsymbol{\Sigma}, \boldsymbol{Q}_{\mathrm{k}}, Q_{\mathrm{i}}) - Q_0^{\mathrm{eq}}, \tag{31}$$

with

$$\Sigma^{\mathrm{eq}}(c\,(\boldsymbol{\Sigma}, \boldsymbol{Q}_{\mathrm{k}}, Q_{\mathrm{i}})) = c^n\, \Sigma^{\mathrm{eq}}(\boldsymbol{\Sigma}, \boldsymbol{Q}_{\mathrm{k}}, Q_{\mathrm{i}}), \qquad c \in \mathbb{R}_+. \tag{32}$$

This constraint is not crucial either and usually, it is fulfilled. Furthermore, all variational constitutive updates proposed so far are based on the aforementioned conditions, cf. [22–28]. It is noteworthy that the class of yield functions spanned by Eqs. (30) – (32) covers almost every plasticity model including those characterized by an anisotropic response such as Barlat-type models, cf. [34].

Based on the yield function, the evolution equations defining the standard dissipative solid are given by

$$\begin{array}{rcl} \boldsymbol{L}^{\mathrm{p}} := \dot{\boldsymbol{F}}^{\mathrm{p}} \cdot \boldsymbol{F}^{\mathrm{p}-1} & = & \lambda\, \partial_{\boldsymbol{\Sigma}}\phi \\ \dot{\alpha}_{\mathrm{i}} & = & \lambda\, \partial_{Q_{\mathrm{i}}}\phi \\ \dot{\boldsymbol{\alpha}}_{\mathrm{k}} & = & \lambda\, \partial_{\boldsymbol{Q}_{\mathrm{k}}}\phi = -\boldsymbol{L}^{\mathrm{p}} \end{array} \tag{33}$$

and the Helmholtz energy (26) yields the thermodynamic forces

$$\begin{array}{rcl} Q_{\mathrm{i}} := -\dfrac{\partial \Psi}{\partial \alpha_{\mathrm{j}}} = -H_{\mathrm{i}}\, \alpha_{\mathrm{i}} \\ \boldsymbol{Q}_{\mathrm{k}} := -\dfrac{\partial \Psi}{\partial \boldsymbol{\alpha}_{\mathrm{k}}} = -H_{\mathrm{k}}\, \boldsymbol{\alpha}_{\mathrm{k}}. \end{array} \tag{34}$$

where Q_{i} and $\boldsymbol{Q}_{\mathrm{k}}$ are stress-like internal variables work conjugate to α_{i} and $\boldsymbol{\alpha}_{\mathrm{k}}$, respectively. Furthermore, since ϕ is a positively homogeneous function of degree n, the dissipation simplifies to

$$\begin{array}{rcl} \mathcal{D} = \boldsymbol{\Sigma} : \boldsymbol{L} - \dot{\Psi} & = & \boldsymbol{\Sigma} : \boldsymbol{L}^{\mathrm{p}} - \dot{\Psi}^{\mathrm{p}} \\ & = & \lambda\, [\partial_{\boldsymbol{\Sigma}}\phi : (\boldsymbol{\Sigma} - \boldsymbol{Q}_{\mathrm{k}}) + \partial_{Q_{\mathrm{i}}}\phi\, Q_{\mathrm{i}}] \\ & = & \lambda\, n\, \Sigma^{\mathrm{eq}}(\boldsymbol{\Sigma} - \boldsymbol{Q}_{\mathrm{k}}, Q_{\mathrm{i}}) \\ & \overset{\phi=0}{=} & n\, \lambda\, Q_o^{\mathrm{eq}} \geq 0. \end{array} \tag{35}$$

Thus, the second law of thermodynamics is indeed fulfilled and even more importantly, the dissipation can be computed explicitly.

Remark 2. The yield surface $\phi = 0$ associated with a yield function fulfilling conditions (30) – (32) can always be re-written as

$$\phi = 0 \;\Leftrightarrow\; \Sigma^{\mathrm{eq}} = Q_0^{\mathrm{eq}} \;\Leftrightarrow\; \sqrt[n]{\Sigma^{\mathrm{eq}}} = \sqrt[n]{Q_0^{\mathrm{eq}}} \;\Leftrightarrow\; \tilde{\phi} := \sqrt[n]{\Sigma^{\mathrm{eq}}} - \sqrt[n]{Q_0^{\mathrm{eq}}} = 0 \tag{36}$$

Clearly, $\sqrt[n]{\Sigma^{\mathrm{eq}}}$ is positively homogeneous of degree one. Hence, without loss of generality, only yield functions being positively homogeneous of degree one are considered in what follows (more precisely, Σ^{eq} is positively homogeneous of degree one). It bears emphasis that, except for a multiplicative constant, both models (corresponding to ϕ or $\tilde{\phi}$) yield the same canonical evolution equations.

3 Numerical implementation

This section representing the main contribution of the present paper is concerned with a novel numerical implementation suitable for standard dissipative solids at finite strains. Analogously to the previous section, the algorithmic formulation is variationally consistent, i.e., all unknown variables follow naturally from minimizing the energy of the considered system. The proposed numerical implementation covers all variational constitutive models which can be found in the literature such as [22–28]. Furthermore and in contrast to the cited works, the advocated model does not rely on any material symmetry and therefore, it can be applied to a broad range of different plasticity theories. Consequently, it represents a significant further development of previous implementations.

This section is organized as follows: In Subsection 3.1 a time discretization transforming the continuous minimization problem (21) into its discrete counterpart is briefly presented. Based on this approximation and as a motivation, the numerical implementation for relatively simple prototype models such as von Mises plasticity theory is carefully analyzed first, see Subsection 3.2. The underlying key idea is to conveniently parameterize the restrictions imposed by the flow rule. Finally, these prototypes are generalized for more complex, possibly anisotropic, plasticity models in Subsection 3.3. An adapted implementation for fully isotropic models is discussed as well.

3.1 Time integration

One of the key ideas of the variationally consistent implementation of standard dissipative solids leading to so-called *variational constitutive updates* is the transformation of the continuous optimization problem (21) into a discrete counterpart. Conceptually, if a consistent time integration is applied, the integrated evolution equations are obtained from the minimization problem

$$(\boldsymbol{F}^{\mathrm{p}}_{n+1}, \boldsymbol{\alpha}_{\mathrm{k}}|_{n+1}, \alpha_{\mathrm{i}}|_{n+1}) = \arg \inf_{\boldsymbol{F}^{\mathrm{p}}_{n+1}, \boldsymbol{\alpha}_{\mathrm{k}}|_{n+1}, \alpha_{\mathrm{i}}|_{n+1}} I_{\mathrm{inc}} \tag{37}$$

with

$$I_{\mathrm{inc}}(\boldsymbol{F}^{\mathrm{p}}_{n+1}, \boldsymbol{\alpha}_{\mathrm{k}}|_{n+1}, \alpha_{\mathrm{i}}|_{n+1}) := \int_{t_n}^{t_{n+1}} \mathcal{E}(\dot{\boldsymbol{\varphi}}, \dot{\boldsymbol{F}}^{\mathrm{p}}, \dot{\boldsymbol{\alpha}})\, \mathrm{d}t = \Psi_{n+1} - \Psi_n + \int_{t_n}^{t_{n+1}} J^*\, \mathrm{d}t \tag{38}$$

cf. Eq. (21). Clearly, I_{inc} depends additionally on the (known) previous time step $(\boldsymbol{F}^{\mathrm{p}}_n, \boldsymbol{\alpha}_{\mathrm{k}}|_n, \alpha_{\mathrm{i}}|_n)$ as well as on the (given) deformation gradient $\boldsymbol{F}_{n+1}$. However, this is not highlighted explicitly.

In line with numerical implementations for standard (not variationally consistent) finite strain plasticity models such as [1, 2], Eq. (37) is approximated by applying a consistent time discretization to the evolution equations. For the sake of concreteness, a first-order fully implicit scheme is adopted. More precisely, with the notation

$$\Delta\lambda := \int_{t_n}^{t_{n+1}} \lambda\, \mathrm{d}t \geq 0 \tag{39}$$

the following approximations are used:

$$\begin{array}{lcl} \boldsymbol{F}^{\mathrm{p}}_{n+1} & = & \exp\left[\Delta\lambda\ \partial_{\boldsymbol{\Sigma}}\phi|_{n+1}\right] \cdot \boldsymbol{F}^{\mathrm{p}}_n \\ \alpha_{\mathrm{i}}|_{n+1} & = & \alpha_{\mathrm{i}}|_n + \Delta\lambda\, \partial_{Q_{\mathrm{i}}}\phi \\ \boldsymbol{\alpha}_{\mathrm{k}}|_{n+1} & = & \boldsymbol{\alpha}_{\mathrm{k}}|_n + \Delta\lambda\ \partial_{\boldsymbol{Q}_{\mathrm{k}}}\phi\big|_{n+1}\,. \end{array} \tag{40}$$

As an alternative to Eq $(40)_c$, the tensor-valued internal variables $\boldsymbol{\alpha}_{\mathrm{k}}$ could be integrated by applying the exponential map, cf. [6], leading to

$$\boldsymbol{\alpha}_{\mathrm{k}}|_{n+1} = \boldsymbol{\alpha}_{\mathrm{k}}|_n \cdot \exp\left[\Delta\lambda\ \partial_{\boldsymbol{Q}_{\mathrm{k}}}\phi\big|_{n+1} \cdot \boldsymbol{\alpha}_{\mathrm{k}}^{-1}\big|_{n+1}\right]. \tag{41}$$

Clearly, with Eq. $(40)_a$, the elastic part of the deformation gradient reads

$$\boldsymbol{F}^{\mathrm{e}}_{n+1} = \boldsymbol{F}^{\mathrm{e}}_{\mathrm{trial}} \cdot \exp\left[-\Delta\lambda\ \partial_{\boldsymbol{\Sigma}}\phi\right] \qquad \boldsymbol{F}^{\mathrm{e}}_{\mathrm{trial}} := \boldsymbol{F}_{n+1} \cdot (\boldsymbol{F}^{\mathrm{p}}_n)^{-1}. \tag{42}$$

It bears emphasis that the time integrations (39)–(41) are indeed consistent and hence, convergence to the analytical solution is guaranteed.

Inserting Eqs. (39), (40) and (42) into Eq. (38), the time integration of $I_{\rm inc}$ yields

$$I_{\rm inc}(\boldsymbol{F}^{\rm p}_{n+1}, \boldsymbol{\alpha}_{\rm k}|_{n+1}, \alpha_{\rm i}|_{n+1}, \Delta\lambda) \approx \Psi_{n+1} - \Psi_n \;+\; \boldsymbol{\Sigma}_{n+1} : \log[\boldsymbol{F}^{\rm p}_{n+1} \cdot (\boldsymbol{F}^{\rm p}_{n})^{-1}] \;+\; [\boldsymbol{Q}_{\rm k} : \partial_{\boldsymbol{Q}_{\rm k}}\phi]|_{n+1}\,\Delta\lambda + [Q_{\rm i}\,\partial_{Q_{\rm i}}\phi]|_{n+1}\,\Delta\lambda. \tag{43}$$

If ϕ (more precisely, $\Sigma^{\rm eq}$) is positively homogeneous of degree one, Eq. (43) simplifies to (cf. Subsection 2.3, Remark 2)

$$I_{\rm inc}(\boldsymbol{F}^{\rm p}_{n+1}, \boldsymbol{\alpha}_{\rm k}|_{n+1}, \alpha_{\rm i}|_{n+1}, \Delta\lambda) = \Psi_{n+1} - \Psi_n + \Delta\lambda\, Q_0^{\rm eq} \tag{44}$$

Since the term Ψ_n shifting the energy depends only on the previous time step, it does not affect the optimization problem (37) or Eq. (44) and hence, it can be neglected. According to the derivation, the potential (43) depends on the considered time integration and hence, uniqueness is only obtained in the limiting case $\Delta t \to 0$.

So far, variational constitutive updates are relatively simple and hence, the respective implementation seems to be straightforward. Unfortunately, this is not the case. The reasons for that are manifold. For instance, a direct minimization of $\Psi_{\rm inc}$ with respect to $\boldsymbol{F}^{\rm p}_{n+1}$ is not admissible, since $\boldsymbol{F}^{\rm p}$ has to comply with physical constraints resulting from the flow rule (and of course, $\det \boldsymbol{F}^{\rm p} > 0$). Furthermore, if plastic loading is considered, the additional restriction $\phi = 0$ has to be enforced relating the stresses (and thus the strains) to the internal variables $\boldsymbol{\alpha}_{\rm k}$ and $\alpha_{\rm i}$. Fortunately, all these problems can be solved efficiently by elaborating a suitable parameterization of the unknown variables. This will be shown in the next subsection.

3.2 Motivation: Implementation of some prototype models

As mentioned before, the main issue associated with variational constitutive updates is the numerical implementation of the minimization problem (37). It depends crucially on a suitable parameterization of the evolution equations. For a better understanding, the algorithmic formulation is briefly presented for four different prototype models first. Each of those fulfills the restrictions summarized in Remark 2. Hence, the functional to be minimized is given by Eq. (44) and the constraint $\phi = 0$ is already included within the optimization, cf. Eq. (44).

3.2.1 Example: Single crystal plasticity

Since single-crystal plasticity (in the sense of Schmid's law) is based on associative evolution equations, the model is defined completely by the respective yield function ϕ. Introducing a slip plane by its corresponding normal vector $\bar{\boldsymbol{n}}$ and the slip direction $\bar{\boldsymbol{m}}$, ϕ is given by

$$\phi(\boldsymbol{\Sigma}, \alpha_{\rm i}) = |\boldsymbol{\Sigma} : (\bar{\boldsymbol{m}} \otimes \bar{\boldsymbol{n}})\,| - Q_{\rm i}(\alpha_{\rm i}) - Q_0^{\rm eq}. \tag{45}$$

Evidently, the vectors $\bar{\boldsymbol{n}}$ and $\bar{\boldsymbol{m}}$ are objects that belong to the intermediate configuration. They are orthogonal to one another and time-independent, i. e.,

$$\bar{\boldsymbol{n}} \cdot \bar{\boldsymbol{m}} = 0 \qquad ||\bar{\boldsymbol{n}}||_2 = ||\bar{\boldsymbol{m}}||_2 = 1. \tag{46}$$

Based on Eq. (45), the evolution equations

$$\boldsymbol{L}^{\rm p} = \tilde{\lambda}\;(\bar{\boldsymbol{m}} \otimes \bar{\boldsymbol{n}})\,, \qquad \text{with} \qquad \tilde{\lambda} = \lambda\;\text{sign}\,[\boldsymbol{\Sigma} : (\bar{\boldsymbol{m}} \otimes \bar{\boldsymbol{n}})]\,, \qquad \dot{\alpha}_{\rm i} = -\lambda \tag{47}$$

are obtained. Hence, only one single variable being λ is unknown. Thus, a suitable parameterization of the time discretized evolution equations reads

$$\boldsymbol{F}^{\rm p}_{n+1} = (\boldsymbol{1} + \Delta\tilde{\lambda}\;\bar{\boldsymbol{m}} \otimes \bar{\boldsymbol{n}}) \cdot \boldsymbol{F}^{\rm p}_{n}, \qquad \alpha_{\rm i}|_{n+1} = \alpha_{\rm i}|_{n} - |\Delta\tilde{\lambda}| \tag{48}$$

and consequently, the minimization problem (35) depends only on the scalar-valued variable $\Delta\tilde{\lambda}$, i.e.,

$$\Delta\tilde{\lambda} := \arg\inf I_{\mathrm{inc}}(\Delta\tilde{\lambda}). \tag{49}$$

It bears emphasis that this property even holds for elastically anisotropic models. This prototype model has already been given earlier by Ortiz et al. [19]. In the cited paper, Ortiz showed that for multiple, simultaneously active, slip systems, variational constitutive updates are significantly more robust and more efficient than classical methods such as the return-mapping scheme. In the cited work and in contrast to the presented paper, the authors started by postulating a flow rule of the type (47) and the yield function followed implicitly from this assumption.

3.2.2 Example: von Mises plasticity theory

For the next prototype model a fully isotropic elastic response is considered. Hence, the Mandel stresses are symmetric. The investigated von Mises yield function including isotropic hardening is given by

$$\phi(\boldsymbol{\Sigma}, \alpha_{\mathrm{i}}) = ||\mathrm{Dev}[\boldsymbol{\Sigma}]|| - Q_{\mathrm{i}}(\alpha_{\mathrm{i}}) - Q_0^{\mathrm{eq}} \tag{50}$$

where $\mathrm{Dev}[\boldsymbol{\Sigma}]$ is the deviator of $\boldsymbol{\Sigma}$ (compare to Subsection (2.3)). Consequently, the evolution equations are computed as

$$\boldsymbol{L}^{\mathrm{p}} = \lambda\, \boldsymbol{M}, \qquad \dot{\alpha}_{\mathrm{i}} = -\lambda, \quad \text{with} \quad \boldsymbol{M} := \frac{\mathrm{Dev}[\boldsymbol{\Sigma}]}{||\mathrm{Dev}[\boldsymbol{\Sigma}]||}. \tag{51}$$

Note that the tensor $\boldsymbol{M}$ shows the properties

$$||\boldsymbol{M}|| = 1, \qquad \mathrm{tr}[\boldsymbol{M}] = 0. \tag{52}$$

Furthermore, if the elastic model is isotropic, the elastic trial strains

$$\boldsymbol{C}^{\mathrm{e}}_{\mathrm{trial}} := (\boldsymbol{F}^{\mathrm{e}}{}_{\mathrm{trial}})^T \cdot \boldsymbol{F}^{\mathrm{e}}{}_{\mathrm{trial}} = \sum_{i=1}^{3} \left(\lambda_i^{\mathrm{etrial}}\right)^2 \; \boldsymbol{N}_i \otimes \boldsymbol{N}_i \tag{53}$$

are coaxial to the (unknown) elastic strains $\boldsymbol{C}^{\mathrm{e}}$ and thus, to the Mandel stresses. As a result, since Eq. (50) is an isotropic tensor function in $\boldsymbol{\Sigma}$, the eigenvectors of the unknown tensor $\boldsymbol{L}^{\mathrm{p}}$ (or $\boldsymbol{M}$) are known in advance, i.e.,

$$\boldsymbol{M} = \sum_{i=1}^{3} \lambda_i^M \; \boldsymbol{N}_i \otimes \boldsymbol{N}_i, \quad \text{with} \quad \sum_{i=1}^{3} \left(\lambda_i^M\right)^2 = 1, \quad \sum_{i=1}^{3} \lambda_i^M = 0, \tag{54}$$

see constraints (52). This, in turn, implies that only two parameters are unknown: the plastic multiplier and one additional parameter defining $\boldsymbol{M}$. Two convenient parameterizations of the restrictions imposed by the flow rule are given below

- Parameterization I depending on $\Delta\lambda_1^{\mathrm{p}}$, $\Delta\lambda_2^{\mathrm{p}}$

$$\begin{aligned} &\Delta\lambda\, \partial_{\boldsymbol{\Sigma}}\phi =: \sum_{i=1}^{3} \Delta\lambda_i^{\mathrm{p}} \; \boldsymbol{N}_i \otimes \boldsymbol{N}_i, \quad \text{with} \quad \Delta\lambda_3^{\mathrm{p}} = -\Delta\lambda_1^{\mathrm{p}} - \Delta\lambda_2^{\mathrm{p}} \\ \Rightarrow \quad &\Delta\alpha_{\mathrm{i}} = \alpha_{\mathrm{i}}|_{n+1} - \alpha_{\mathrm{i}}|_n = -\sqrt{\sum_{i=1}^{3} (\Delta\lambda_i^{\mathrm{p}})^2} \end{aligned} \tag{55}$$

- Parameterization II depending on θ and a; ([46])

$$\begin{array}{rcl} \lambda_i^M & = & \sqrt{\dfrac{2}{3}}\,\sin\left[\dfrac{2\,\alpha_i\,\pi}{3}-\theta\right], \quad \alpha_i=1,2,3 \quad \text{cf. Eq. (54)} \\ \Delta\lambda & = & a^2\geq 0 \end{array} \tag{56}$$

A similar model was recently proposed in [28]. However, it is noteworthy that in contrast to the numerical formulation discussed in [28], the presented prototype can easily include coupled isotropic/kinematic hardening and therefore, it is more general and represents a further development.

3.2.3 Example: Associative Drucker-Prager plasticity model

This model is defined by the yield function

$$\phi(\boldsymbol{\Sigma},\alpha_{\rm i}) = \kappa\,\text{tr}[\boldsymbol{\Sigma}] + ||\text{Dev}[\boldsymbol{\Sigma}]|| - Q_{\rm i}(\alpha_{\rm i}) - Q_0^{\rm eq}. \tag{57}$$

with κ being a material parameter. Eq. (57) yields the associative evolution equations

$$\boldsymbol{L}^{\rm p} = \lambda\;(\kappa\,\boldsymbol{1}+\boldsymbol{M})\,, \quad \dot{\alpha}_{\rm i} = -\lambda \tag{58}$$

where $\boldsymbol{M}$ is given by Eq. (54). Clearly, if the elastic response is fully isotropic, $\boldsymbol{M}$ and λ can again conveniently be parameterized by Eq. (56). It bears emphasis that the prototype presented in this subsection was not published in a variationally consistent manner before.

3.2.4 Example: Rankine plasticity model

The final example is associated with Rankine plasticity theory. The respective yield function is postulated to be

$$\phi(\boldsymbol{\Sigma},\alpha_{\rm i}) = \Sigma_{\max}(\boldsymbol{\Sigma}) - Q_{\rm i}(\alpha_{\rm i}) - Q_0^{\rm eq}. \tag{59}$$

Here, $\Sigma_{\max}(\boldsymbol{\Sigma})$ is the maximum principal Mandel stress. Considering a fully isotropic elastic behavior, Eq. (59) results in the normality evolution equations

$$\boldsymbol{L}^{\rm p} = \lambda\;\boldsymbol{N}_{\max}\otimes\boldsymbol{N}_{\max}, \quad \dot{\alpha}_{\rm i} = -\lambda. \tag{60}$$

with $\boldsymbol{N}_{\max}$ denoting the eigenvector corresponding to $\Sigma_{\max}$. Note that $\boldsymbol{N}_{\max}$ is known in advance, if a fully isotropic model is chosen (and the Baker-Ericksen inequalities hold). Hence, the only unknown parameter is λ which can conveniently be parameterized by $\Delta\lambda = a^2$. In line with the models summarized before, a variationally consistent Rankine model has not been advocated in the literature before.

3.3 An efficient variational constitutive update

As shown in the previous subsections, the numerical computation of the optimization problem (43) strongly depends on a convenient parameterization of the evolution equations and the flow rule. Such a parameterization which can be applied to a broad range of different constitutive models will be discussed in Subsection 3.3.1. Subsequently, the simplifications holding for fully isotropic models (elastic and plastic) are addressed in Subsection 3.3.2 leading to an adapted, tuned variational constitutive update. Both implementations significantly extend previous works on variational constitutive updates such as [22–28].

3.3.1 The general case

As evident from the prototype models, a convenient parameterization of the flow rule and the evolution equations depends strongly on the considered plasticity model, i.e., the yield function. For deriving a parameterization which holds for a broad range of different models, the (unknown) arguments $\boldsymbol{F}^{\mathrm{p}}_{n+1}$, $\boldsymbol{\alpha}_{\mathrm{k}}|_{n+1}$, $\alpha_{\mathrm{i}}|_{n+1}$ and $\Delta\lambda$ entering the incrementally defined potential (43) are replaced by a more suitable representation. More precisely,

$$I_{\mathrm{inc}} = I_{\mathrm{inc}}(\boldsymbol{M}, \boldsymbol{H}_{\mathrm{k}}, H_{\mathrm{i}}, \Delta\lambda) \tag{61}$$

with

$$\boldsymbol{M} := \partial_{\boldsymbol{\Sigma}}\phi, \quad \boldsymbol{H}_{\mathrm{k}} := \partial_{\boldsymbol{Q}_{\mathrm{k}}}\phi, \quad H_{\mathrm{i}} := \partial_{Q_{\mathrm{i}}}\phi. \tag{62}$$

Accordingly, $\boldsymbol{M}$, $\boldsymbol{H}_{\mathrm{k}}$ and H_{i} are the flow direction, the kinematic hardening direction and the isotropic hardening gradient, respectively. Clearly, $\boldsymbol{M}$, $\boldsymbol{H}_{\mathrm{k}}$ and H_{i} cannot be chosen arbitrarily, but have to comply with the restrictions imposed by the constitutive model. For this reason, the aforementioned directions are parameterized as follows:

$$\boldsymbol{M} = \boldsymbol{M}(\tilde{\boldsymbol{\Sigma}}) := \partial_{\boldsymbol{\Sigma}}\phi|_{\tilde{\boldsymbol{\Sigma}}} \tag{63}$$

$$\boldsymbol{H}_{\mathrm{k}} = \boldsymbol{H}_{\mathrm{k}}(\tilde{\boldsymbol{Q}}_{\mathrm{k}}) := \partial_{\boldsymbol{Q}_{\mathrm{k}}}\phi\big|_{\tilde{\boldsymbol{Q}}_{\mathrm{k}}} \tag{64}$$

$$H_{\mathrm{i}} = H_{\mathrm{i}}(\tilde{Q}_{\mathrm{i}}) := \partial_{Q_{\mathrm{i}}}\phi|_{\tilde{Q}_{\mathrm{i}}} \tag{65}$$

$$\Delta\lambda = \Delta\lambda(a) := a^2 \tag{66}$$

Here, the unknowns $\tilde{\boldsymbol{\Sigma}}$, $\tilde{\boldsymbol{Q}}_{\mathrm{k}}$ and $\tilde{Q}_{\mathrm{i}}$ denote pseudo stresses, a pseudo backstress and a pseudo stress-like hardening variable. It has to be emphasized that these pseudo variables are not identical to their physical counterparts in general, i.e.,

$$\tilde{\boldsymbol{\Sigma}} \neq \boldsymbol{\Sigma}, \quad \tilde{\boldsymbol{Q}}_{\mathrm{k}} \neq \boldsymbol{Q}_{\mathrm{k}}, \quad \tilde{Q}_{\mathrm{i}} \neq Q_{\mathrm{i}}. \tag{67}$$

More precisely, the variables $\tilde{\boldsymbol{\Sigma}}$, $\tilde{\boldsymbol{Q}}_{\mathrm{k}}$ and $\tilde{Q}_{\mathrm{i}}$ only define the flow and hardening directions. Thus, they are related to their physical counterparts by

$$\boldsymbol{M}(\tilde{\boldsymbol{\Sigma}}) = \boldsymbol{M}(\boldsymbol{\Sigma}), \quad \boldsymbol{H}_{\mathrm{k}}(\tilde{\boldsymbol{Q}}_{\mathrm{k}}) = \boldsymbol{H}_{\mathrm{k}}(\boldsymbol{Q}_{\mathrm{k}}), \quad H_{\mathrm{i}}(\tilde{Q}_{\mathrm{i}}) = H_{\mathrm{i}}(Q_{\mathrm{i}}). \tag{68}$$

As a result and in contrast to the original parameterization, Eqs. (63)–(66) automatically fulfill the restrictions associated with the considered constitutive model. For instance, in case of von Mises plasticity,

$$\phi = ||\mathrm{Dev}\boldsymbol{\Sigma}|| - Q_{\mathrm{i}}(\alpha_{\mathrm{i}}) - Q_0^{\mathrm{eq}} \quad \Rightarrow \quad \boldsymbol{M}(\tilde{\boldsymbol{\Sigma}}) = \frac{\mathrm{Dev}[\tilde{\boldsymbol{\Sigma}}]}{||\mathrm{Dev}[\tilde{\boldsymbol{\Sigma}}]||} \tag{69}$$

and thus the constraints,

$$\mathrm{tr}[\boldsymbol{M}] = 0, \qquad \boldsymbol{M} : \boldsymbol{M} = 1, \quad \forall\tilde{\boldsymbol{\Sigma}} \tag{70}$$

are naturally enforced. The same holds for the evolution equations corresponding to hardening. Obviously, additional constraints such as $Q_{\mathrm{i}} \geq 0$ can be easily taken into account as well. Inserting Eqs. (63)–(66) into Eq. (61) leads to

$$I_{\mathrm{inc}} = I_{\mathrm{inc}}(\boldsymbol{X}), \quad \text{with} \quad \boldsymbol{X} = [\tilde{\boldsymbol{\Sigma}}, \tilde{\boldsymbol{Q}}_{\mathrm{k}}, Q_{\mathrm{i}}, a] \quad \Rightarrow \quad \dim[\boldsymbol{X}] = 20 \tag{71}$$

Finally, the unknowns $\boldsymbol{X}$ can be computed from the constrained optimization scheme

$$\boldsymbol{X} = \arg \inf_{\boldsymbol{X}, \phi \leq 0} I_{\rm inc}(\boldsymbol{X}). \tag{72}$$

For that purpose, by now standard algorithms can be applied, cf. [47]. Evidently, the choice of a suited method depends strongly on the possibly non-linear constraint $\phi = 0$ (plastic loading). In the following paragraph, attention is turned on a certain class of plasticity models. This class contains a large number of important constitutive laws.

In this paragraph, an efficient solution scheme for optimization problem (72) is developed. It is restricted to yield functions such as those described in Subsection 2.3, cf. Remark 2. As mentioned before, almost every plasticity model falls into this range. According to Eq. (35) and Remark 2, in this case, the cumbersome non-linear constraint $\phi = 0$ can be directly included in the dissipation resulting in $\mathcal{D} = \lambda \; Q_0^{\rm eq} \geq 0$. Furthermore, since for this class of models the evolution equations yield

$$\boldsymbol{H}_{\rm k} = -\boldsymbol{M}, \quad \text{and} \quad \dot{\alpha}_{\rm i} = -\lambda, \tag{73}$$

the non-linear constrained optimization problem (72) can be significantly simplified, i.e.,

$$\boldsymbol{X} = \arg \inf_{\boldsymbol{X}} I_{\rm inc}(\boldsymbol{X}), \quad \text{with} \quad I_{\rm inc} = \Psi_{n+1}(\boldsymbol{X}) - \Psi_n + Q_0^{\rm eq} \; \Delta\lambda \tag{74}$$

with the unknowns being

$$\boldsymbol{X} = [\tilde{\boldsymbol{\Sigma}}, a] \quad \Rightarrow \quad \dim[\boldsymbol{X}] = 10. \tag{75}$$

As a result, the complexity of the problem is reduced by a factor of 2. The unconstrained minimization problem (74) can be solved in a standard manner, e.g., by employing gradient-type schemes, cf. [48]. Applying the time integrations (40) and subsequently, using the derivatives

$$\frac{\partial \Psi^{\rm e}}{\partial \Delta\lambda} = - \left[(\boldsymbol{F}^{\rm e}_{\rm trial})^T \cdot \frac{\partial \Psi^{\rm e}}{\partial \boldsymbol{F}^{\rm e}} \right] : D\exp\left[- \Delta\lambda \; \partial_{\boldsymbol{\Sigma}} \phi|_{\tilde{\boldsymbol{\Sigma}}} \right] : \partial_{\boldsymbol{\Sigma}} \phi|_{\tilde{\boldsymbol{\Sigma}}} \tag{76}$$

$$\frac{\partial \Psi^{\rm e}}{\partial \tilde{\boldsymbol{\Sigma}}} = - \left[(\boldsymbol{F}^{\rm e}_{\rm trial})^T \cdot \frac{\partial \Psi^{\rm e}}{\partial \boldsymbol{F}^{\rm e}} \right] : D\exp\left[- \Delta\lambda \; \partial_{\boldsymbol{\Sigma}} \phi|_{\tilde{\boldsymbol{\Sigma}}} \right] : \partial^2_{\boldsymbol{\Sigma}} \phi\big|_{\tilde{\boldsymbol{\Sigma}}} \; \Delta\lambda \tag{77}$$

$$\begin{aligned} \frac{\partial \Psi^{\rm p}}{\partial \Delta\lambda} &= \frac{\partial \Psi^{\rm p}}{\partial \alpha_{\rm i}} \frac{\partial \alpha_{\rm i}}{\partial \Delta\lambda} + \frac{\partial \Psi^{\rm p}}{\partial \boldsymbol{\alpha}_{\rm k}} : \frac{\partial \boldsymbol{\alpha}_{\rm k}}{\partial \Delta\lambda} \\ &= Q_{\rm i} + \boldsymbol{Q}_{\rm k} : \partial_{\boldsymbol{\Sigma}} \phi|_{\tilde{\boldsymbol{\Sigma}}}, \end{aligned} \tag{78}$$

$$\frac{\partial \Psi^{\rm p}}{\partial \tilde{\boldsymbol{\Sigma}}} = \frac{\partial \Psi^{\rm p}}{\partial \boldsymbol{\alpha}_{\rm k}} : \frac{\partial \boldsymbol{\alpha}_{\rm k}}{\partial \tilde{\boldsymbol{\Sigma}}} = \Delta\lambda \; \boldsymbol{Q}_{\rm k} : \partial^2_{\boldsymbol{\Sigma}} \phi\big|_{\tilde{\boldsymbol{\Sigma}}} \tag{79}$$

the gradient of $I_{\rm inc}$ can be computed in a straightforward manner. In line with Eq. (63), the elastic part of the deformation gradient is computed by means of

$$\boldsymbol{F}^{\rm e}_{n+1} = \boldsymbol{F}^{\rm e}_{\rm trial} \cdot \exp\left[-a^2 \;\; \partial_{\boldsymbol{\Sigma}} \phi|_{\tilde{\boldsymbol{\Sigma}}} \right]. \tag{80}$$

Clearly, in case of an exponential approximation of the evolution equations for $\boldsymbol{\alpha}_{\rm k}$, the gradient has to be modified accordingly. In Eqs. (76) and (77), the derivative of the exponential mapping

$$D\exp[\boldsymbol{A}] := \frac{\partial \exp[\boldsymbol{A}]}{\partial \boldsymbol{A}} \tag{81}$$

can be computed in a standard fashion, e.g. [49, 50]. The examples presented in the next section have been computed by applying a globally convergent Newton-type iteration, cf. [48]. For that purpose, the second derivatives of $I_{\rm inc}$ are required. Although they result in relatively lengthy equations, they can be calculated in a straightforward manner. Therefore, the Hessian of $I_{\rm inc}$ is omitted.

Remark 3. According to Eqs. (76) and (79), stability of $I_{\rm inc}$ with respect to the plastic multiplier $\Delta\lambda$ reads

$$\left.\frac{\partial I}{\partial \Delta\lambda}\right|_{\Delta\lambda=0} = -\left[\boldsymbol{\Sigma} : \partial_{\boldsymbol{\Sigma}}\phi + Q_{\rm i} + \boldsymbol{Q}_{\rm k} : \partial_{\boldsymbol{\Sigma}}\phi + Q_0^{\rm eq}\right]|_{\rm trial} = -\phi_{\rm trial} > 0 \tag{82}$$

which coincides with the classical (discrete) unloading condition $\phi_{\rm trial} \leq 0$. It is noteworthy that this property is fulfilled for any consistent time integration.

Remark 4. Using a parameterization of the type $\Delta\lambda = a^2 \geq 0$, the functional $I_{\rm inc}$ shows an extremum at $a = 0$ (if $Q_{\rm i}(t_n) = 0$ and $\boldsymbol{Q}_{\rm k}(t_n) = \boldsymbol{0}$). Hence, if classical gradient-type optimization schemes are employed, a non-vanishing initial value $a = \text{TOL} > 0$ should be used for a plastic loading step. However, within the current implementation, the unloading condition (82) (stability condition) is first checked. Only if it is violated, a plastic corrector, i.e., the optimization problem, is considered.

Remark 5. If the yield function (more precisely, $\Sigma^{\rm eq}$) is positively homogeneous of degree n, it can always be re-written into a positively homogeneous of degree one counterpart (see Remark 2). In this case, the flow rule for $\boldsymbol{L}^{\rm p}$ is split into an amplitude λ and a direction $\partial_{\boldsymbol{\Sigma}}\phi$. This property is crucial for the proposed variational update. This can be seen directly by considering a simple counter-example given by a yield function which is positively homogeneous of degree two (such as $\phi = ||\text{Dev}[\boldsymbol{\Sigma}]||^2 - (Q_0^{\rm eq})^2$). For this case, consider two states related to one another according to $\tilde{\boldsymbol{\Sigma}}^{(2)} = c\ \tilde{\boldsymbol{\Sigma}}^{(1)}$ and $\Delta\lambda^{(2)} = 1/c\ \Delta\lambda^{(1)}$. Clearly, they result in the same integrated flow rule, i.e., $\Delta\boldsymbol{L}^{\rm p} = \Delta\lambda^{(1)}\partial_{\boldsymbol{\Sigma}}\phi|_{\tilde{\boldsymbol{\Sigma}}^{(1)}} = \Delta\lambda^{(2)}\partial_{\boldsymbol{\Sigma}}\phi|_{\tilde{\boldsymbol{\Sigma}}^{(2)}}$. However, the respective dissipations yield $\int_{\Delta t}\mathcal{D}\ {\rm d}t = 2\ \Delta\lambda^{(i)}\ (Q_0^{\rm eq})^2$. Hence, in terms of energy minimization, the non-physical solution $c \to \infty$ implying $\int_{\Delta t}\mathcal{D}\ {\rm d}t = 0$ is preferable. Clearly, such a non-physical solution cannot occur, if the yield function is positively homogeneous of degree one. It bears emphasis that the advocated implementation can indeed be extended to the more general case in a relatively simple manner, i.e., positively homogeneous of degree n . However according to Remark 2, this is not required.

Remark 6. The presented framework is restricted to rate-independent plasticity. However, the extensions necessary for rate-dependent effects such as viscoplasticity are straightforward. More precisely, and in line with [19], an additional term depending on the rate of the inelastic strains has simply to be added to Eq. $(74)_2$ in this case. Clearly, such a modification does not affect the advocated parameterization and hence, the algorithm has only to be modified slightly.

3.3.2 Fully isotropic models

In this subsection, a tuned version of the novel optimization scheme discussed before is given. It is based on the same assumptions as made before (Subsection 2.3). Additionally, the stored energy potential Ψ as well as the yield function are postulated to be isotropic tensor functions (without structural tensors). For such models, it is straightforward to show that all tensors are

coaxial. More precisely,

$$\begin{aligned}
\boldsymbol{C}^{\mathrm{e}}_{\mathrm{trial}} &= \sum_{i=1}^{3} \left(\lambda_i^{\mathrm{etrial}}\right)^2 \; \boldsymbol{N}_i \otimes \boldsymbol{N}_i \\
\boldsymbol{C}^{\mathrm{e}} &= \sum_{i=1}^{3} \left(\lambda_i\right)^2 \; \boldsymbol{N}_i \otimes \boldsymbol{N}_i \\
\boldsymbol{\Sigma} &= \sum_{i=1}^{3} \Sigma_i \; \boldsymbol{N}_i \otimes \boldsymbol{N}_i \\
\partial_{\boldsymbol{\Sigma}}\phi &= \sum_{i=1}^{3} \partial_{\Sigma_i}\phi \; \boldsymbol{N}_i \otimes \boldsymbol{N}_i
\end{aligned} \tag{83}$$

Consequently, the optimization scheme (74) reduces to

$$\boldsymbol{X} = \arg\inf_{\boldsymbol{X}} I_{\mathrm{inc}}(\boldsymbol{X}), \quad \text{with} \quad I_{\mathrm{inc}} = \Psi_{n+1}(\boldsymbol{X}) - \Psi_n + Q_0^{\mathrm{eq}}\, a^2 \tag{84}$$

with the unknowns being

$$\boldsymbol{X} = [\tilde{\Sigma}_1, \tilde{\Sigma}_2, \tilde{\Sigma}_3, a] \quad \Rightarrow \quad \dim[\boldsymbol{X}] = 4. \tag{85}$$

Again, it is strictly distinguished between principal Mandel stresses Σ_i and their pseudo counterparts $\tilde{\Sigma}_i$ which define the flow direction. Using the spectral decomposition of the total differential of the exponential mapping (for fixed eigenvectors $\boldsymbol{N}_i$)

$$\begin{aligned}
\mathrm{d}\left\{\exp\left[-\Delta\lambda\; \partial_{\boldsymbol{\Sigma}}\phi\right]\right\} = \; & -\left\{\sum_{i=1}^{3} \partial_{\Sigma_i}\phi \; \exp[-\Delta\lambda\; \partial_{\Sigma_i}\phi] \; \boldsymbol{N}_i \otimes \boldsymbol{N}_i\right\} \mathrm{d}\Delta\lambda \\
& -\sum_{j=1}^{3} \left\{\sum_{i=1}^{3} \Delta\lambda\; \partial^2_{\Sigma_i\Sigma_j}\phi \; \exp[-\Delta\lambda\; \partial_{\Sigma_i}\phi] \; \boldsymbol{N}_i \otimes \boldsymbol{N}_i\right\} \mathrm{d}\Sigma_j,
\end{aligned} \tag{86}$$

together with

$$\left[(\boldsymbol{F}^{\mathrm{e}}_{\mathrm{trial}})^T \cdot \frac{\partial \Psi^{\mathrm{e}}}{\partial \boldsymbol{F}^{\mathrm{e}}}\right] = \sum_{i=1}^{3} P_i^{\mathrm{e}} \; \lambda_i^{\mathrm{etrial}} \; \boldsymbol{N}_i \otimes \boldsymbol{N}_i, \tag{87}$$

the gradients (76) – (79) simplify greatly, i.e.,

$$\frac{\partial \Psi^{\mathrm{e}}}{\partial \Delta\lambda} = -\sum_{i=1}^{3} P_i^{\mathrm{e}} \; \lambda_i^{\mathrm{etrial}} \; \partial_{\Sigma_i}\phi|_{\tilde{\Sigma}_i} \; \exp(-\Delta\lambda \; \partial_{\Sigma_i}\phi|_{\tilde{\Sigma}_i}) \tag{88}$$

$$\frac{\partial \Psi^{\mathrm{e}}}{\partial \tilde{\Sigma}_j} = -\sum_{i=1}^{3} P_i^{\mathrm{e}} \; \lambda_i^{\mathrm{etrial}} \; \Delta\lambda \; \partial^2_{\Sigma_i\Sigma_j}\phi\Big|_{\tilde{\Sigma}_i} \; \exp[-\Delta\lambda \; \partial_{\Sigma_i}\phi|_{\tilde{\Sigma}_i}] \tag{89}$$

$$\frac{\partial \Psi^{\mathrm{p}}}{\partial \Delta\lambda} = Q_{\mathrm{i}} + \boldsymbol{Q}_{\mathrm{k}} : \left(\sum_{i=1}^{3} \partial_{\Sigma_i}\phi|_{\tilde{\Sigma}_i} \; \boldsymbol{N}_i \otimes \boldsymbol{N}_i\right) \tag{90}$$

$$\frac{\partial \Psi^{\mathrm{p}}}{\partial \tilde{\Sigma}_j} = \Delta\lambda \; \boldsymbol{Q}_{\mathrm{k}} : \left(\sum_{i=1}^{3} \partial_{\Sigma_i\Sigma_j}\phi^2\big|_{\tilde{\Sigma}_i} \; \boldsymbol{N}_i \otimes \boldsymbol{N}_i\right) \tag{91}$$

Here, P_i^{e} represents the eigenvalues of $\boldsymbol{P}^{\mathrm{e}} := \partial_{\boldsymbol{F}^{\mathrm{e}}}\Psi$. If a Newton-type iteration is to be applied for solving the nonlinear optimization scheme, the second derivatives of I_{inc} are needed. As in

the more general case discussed in the previous subsection, they can be computed in a straightforward manner. Consequently, they are omitted here. Clearly, analogously to the standard return-mapping algorithm formulated in principal axes, the now non-vanishing derivatives of the eigenvectors $\boldsymbol{N}_i$ have to be considered, i.e., $\mathrm{d}(\boldsymbol{N}_i \otimes \boldsymbol{N}_i) \neq \boldsymbol{0}$, cf. [1]. It bears emphasis that the proposed implementation for fully isotropic models significantly extends the recent work [28] which can only be applied to von Mises type models with isotropic hardening.

4 Numerical examples

The versatility and the performance of the proposed constitutive update are demonstrated by means of selected numerical examples. In Subsection 4.1 a fully orthotropic Hill-type model is analyzed numerically, while an orthotropic Barlat-type model is investigated in Subsection 4.2. In both subsections, mechanical problems characterized by homogeneous stress states are considered (simple tension, simple shear). Finally, a more complex example being a strip with a circular hole is computed in Subsection 4.3.

4.1 An orthotropic Hill-type model

In this subsection, a fully orthotropic Hill-type model is analyzed by applying the variational constitutive updates as presented before. The orthotropic model is characterized by a quadratic elastic stored energy potential of the type

$$\begin{aligned}\Psi^{\mathrm{e}} = \quad & \frac{1}{2}\,\lambda\,J_1^2 + \mu\,J_2 + \frac{1}{2}\,\alpha_1\,J_4^2 + \frac{1}{2}\,\alpha_2\,J_6^2 + 2\,\alpha_3\,J_5 + 2\,\alpha_4\,J_7 \\ + \quad & \alpha_5\,J_4\,J_1 + \alpha_6\,J_6\,J_1 + \alpha_7\,J_4\,J_6.\end{aligned} \tag{92}$$

Here, J_i are the invariants

$$\begin{gathered} J_1 := \mathrm{tr}[\boldsymbol{E}], \quad J_2 := \mathrm{tr}[\boldsymbol{E}^2], \\ J_4 := \mathrm{tr}[\boldsymbol{M}^{(1)} \cdot \boldsymbol{E}], \quad J_5 := \mathrm{tr}[\boldsymbol{M}^{(1)} \cdot \boldsymbol{E}^2], \quad J_6 := \mathrm{tr}[\boldsymbol{M}^{(2)} \cdot \boldsymbol{E}], \quad J_7 := \mathrm{tr}[\boldsymbol{M}^{(2)} \cdot \boldsymbol{E}^2] \end{gathered} \tag{93}$$

depending on the Green-Lagrange strain tensor $\boldsymbol{E}$ and so-called structural tensors $\boldsymbol{M}^{(i)} = \boldsymbol{m}_i \otimes \boldsymbol{m}_i$ where $\boldsymbol{m}_i$ span an orthonormal basis. In this section, the bases $\boldsymbol{m}_i$ are assumed to be of the type $\boldsymbol{m}_1 = [\cos\beta; \sin\beta; 0]$, $\boldsymbol{m}_2 = [-\sin\beta; \cos\beta; 0]$ and $\boldsymbol{m}_3 = [0; 0; 1]$. The angle β is set to $\beta = 10^\circ$. The material parameters defining the elastic response are summarized in Tab. 1.

	λ	μ	α_1	α_2	α_3	α_4	α_5	α_6	α_7
ortho.	67.25	81.00	67.46	-3.10	-15.00	0.00	2.00	-7.55	0.98
iso.	67.25	81.00	0	0	0	0	0	0	0

Table 1: Hill-type model: material parameters (GPa) defining the orthotropic and the isotropic elastic response according to Eq. (92), cf. [51]

The elastic space is defined by a Hill-type yield function, i.e.,

$$\phi(\boldsymbol{\Sigma}, \boldsymbol{Q}_{\mathrm{k}}, Q_{\mathrm{i}}) := \Sigma^{\mathrm{eq}}(\boldsymbol{\Sigma} - \boldsymbol{Q}_{\mathrm{k}}) - Q_{\mathrm{i}} - Q_o^{\mathrm{eq}}, \tag{94}$$

with

$$\Sigma^{\mathrm{eq}}(\boldsymbol{A}) := \sqrt{\boldsymbol{A} : \mathbb{H} : \boldsymbol{A}},\ \mathbb{H} = \mathbb{P}_{\mathrm{Dev}} : \mathbb{D} : \mathbb{P}_{\mathrm{Dev}},\ \mathbb{P}_{\mathrm{Dev}} := \mathbb{I} - \frac{1}{3}\,\boldsymbol{1} \otimes \boldsymbol{1} \tag{95}$$

Thus, different material symmetries can be incorporated by choosing the 4th-order weighting tensor $\mathbb{D}$ accordingly. For $\mathbb{D} = \mathbb{I}$ the isotropic von Mises model is obtained. In the numerical examples presented in this section, a fully isotropic and an orthotropic yield function are considered. The corresponding non-vanishing components of the weighting tensor $\mathbb{D}$ are given in Tab. 2. It can be easily checked, that the coefficients $\mathbb{D}_{ijkl}$ define a convex space of admissible

	$\mathbb{D}_{1111}$	$\mathbb{D}_{2121}$	$\mathbb{D}_{3131}$	$\mathbb{D}_{1212}$	$\mathbb{D}_{2222}$	$\mathbb{D}_{3232}$	$\mathbb{D}_{1313}$	$\mathbb{D}_{2323}$	$\mathbb{D}_{3333}$
ortho.	0.918887	4.18388	6.25	4.18388	-0.516313	5.0625	6.25	5.0625	5.84076
iso.	1	1	1	1	1	1	1	1	1

Table 2: Hill-type model: non-vanishing components of the weighting tensor $\mathbb{D}$ for an orthotropic as well as for an isotropic equivalent stress Σ^{eq} according to Eq. (95) (see also [51]); $Q_0^{\text{eq}} = 0.585$ GPa

elastic stresses.

Different hardening models are analyzed. Each of them falls into the class defined by Eqs. (27) and (29). The respective material parameters are listed below.

	H_i	H_k
No hardening	0	0
Isotropic	1.0	0
Kinematic	0.0	1.0
Combined	0.5	0.5

Table 3: Hill-type model: material parameters (GPa) for different hardening models according to Eqs. (27) and (29)

4.1.1 Shear test

At first, a simple shear test is investigated. More precisely, the following stress states are analyzed:

$$\boldsymbol{P} = P_{12}\, \boldsymbol{e}_1 \otimes \boldsymbol{e}_2, \quad \boldsymbol{P} = P_{13}\, \boldsymbol{e}_1 \otimes \boldsymbol{e}_3, \quad \boldsymbol{P} = P_{23}\, \boldsymbol{e}_2 \otimes \boldsymbol{e}_3. \tag{96}$$

Here and henceforth, $\boldsymbol{e}_i$ denote the standard cartesian basis. It bears emphasis that the vectors $\boldsymbol{e}_i$ are not identical to those defining the material symmetry, i.e., $\boldsymbol{e}_i \neq \boldsymbol{m}_i$. In contrast to purely displacement-driven problems, Eqs. (96) represent a Neumann problem. For the computation of the solution, a Newton-type iteration has been implemented. By doing so, the linearizations of the algorithm can be checked.

For a careful analysis of the fully orthotropic model (orthotropic elastic and plastic response), the three different simple shear tests according to Eqs. (96) are compared to the fully isotropic model. The computed results are shown in Fig. 1. Here, isotropic hardening has been assumed, cf. Tab. 3. It is evident from Fig. 1 that the model is indeed highly anisotropic. More precisely, depending on the loading direction, elastic yielding starts at different stress states. Furthermore, since the investigated problem is highly coupled, hardening is affected by the loading direction as well. However, this dependency is less pronounced.

For kinematic hardening (see Tab. 3), the stress-strain-diagrams corresponding to the simple shear test are shown in Fig. 2. Again, the orthotropic material behavior is obvious. However, in

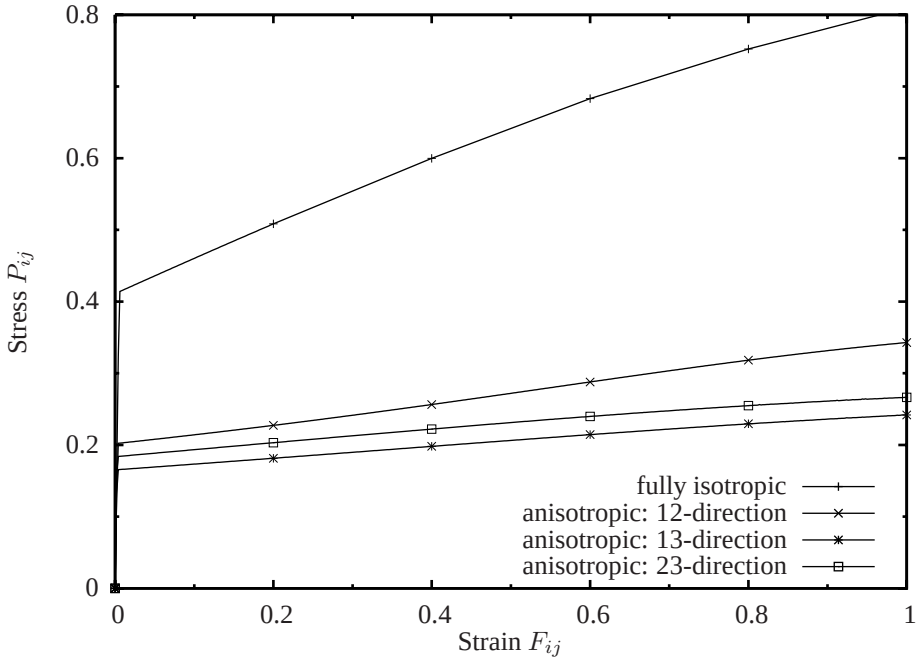

Figure 1: Hill-type model – monotonic shear test: stress-strain diagram associated with isotropic hardening ($H_i = 1.0$, $H_k = 0.0$); results predicted by the fully anisotropic model (elastic and plastic) depending on the loading direction. For the sake of comparison, the response computed from the isotropic model (elastic and plastic) is shown as well.

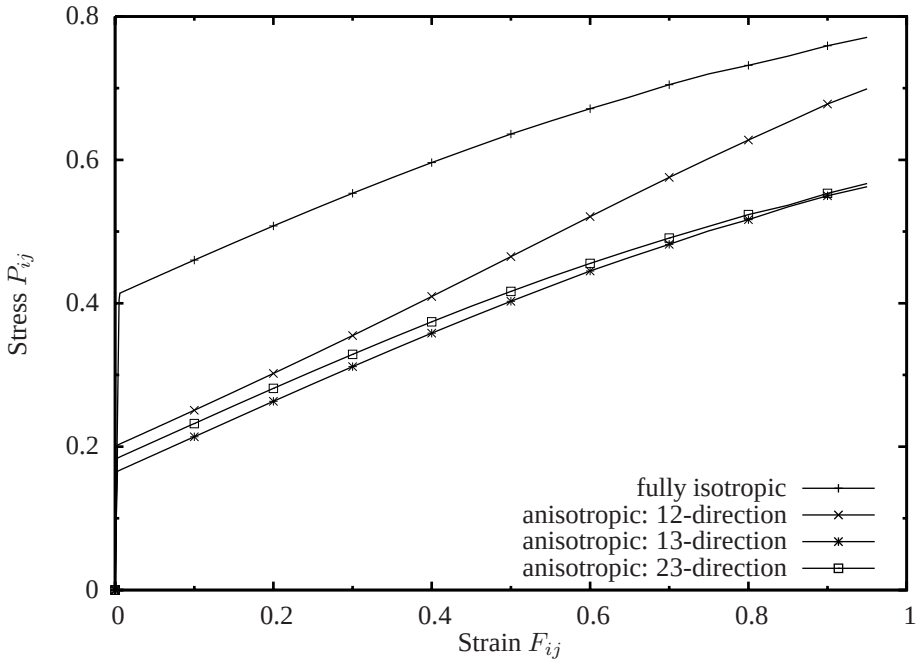

Figure 2: Hill-type model – monotonic shear test: stress-strain diagram associated with kinematic hardening ($H_i = 0.0$, $H_k = 1.0$); results predicted by the fully anisotropic model (elastic and plastic) depending on the loading direction. For the sake of comparison, the response computed from the isotropic model (elastic and plastic) is shown as well.

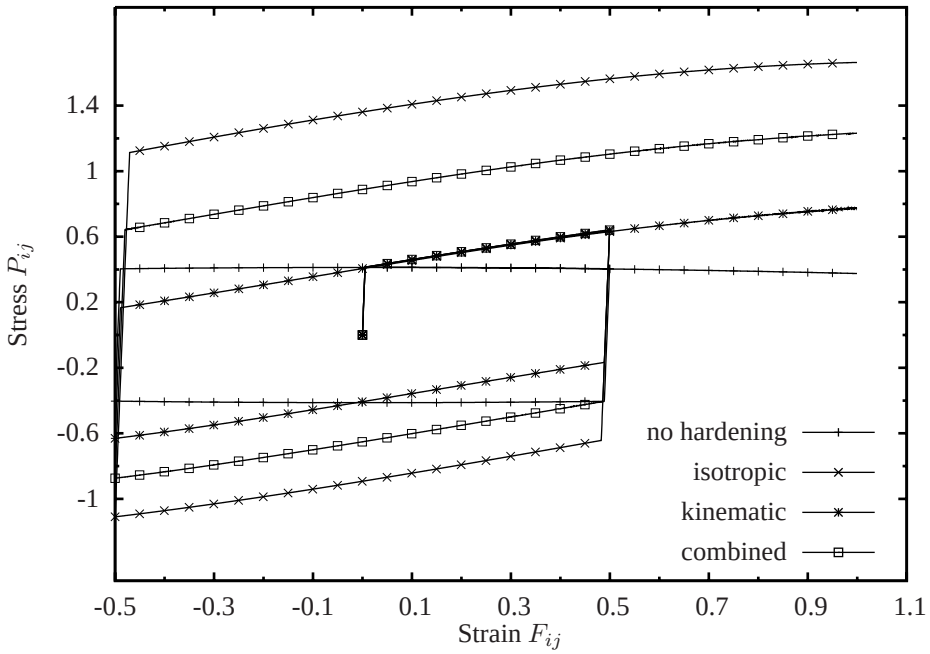

Figure 3: Hill-type model – cyclic shear test: stress-strain diagram associated with a fully isotropic formulation (elastic and plastic) depending on the hardening model

contrast to isotropic hardening, kinematic hardening induces an additional degree of coupling. For this reason, the differences in the $P-F$ diagrams are more pronounced compared to Fig. 1.

Next, the influence of different hardening models is investigated. For that purpose, cycling loading is considered. The computed responses for the fully isotropic model (elastically isotropic and isotropic yield function) are summarized in Fig. 3. As expected, during the first stage (loading) all hardening approaches lead to the same results, since the harding moduli are identical, cf. Tab. 3. Furthermore, after unloading and an additional re-loading step, the classical hysteresis can be observed. Although the applied strains are relatively large, Fig. 3 agrees reasonably with the linearized theory. In summary, it can be verified that the proposed variational constitutive update works correctly.

Next, the cyclic simple shear test is re-analyzed by adopting the fully anisotropic constitutive model (elastically orthotropic and orthotropic yield function). The computed stress-strain responses are given in Fig. 4. According to Fig. 4 and in contrast to the fully isotropic model (see Fig. 3), the $P-F$ diagrams are now even different during the first loading stage. Clearly, this is a direct consequence, of the anisotropy of the material. Although the simple shear test represents one of the simplest mechanical problems, it is relatively difficult to estimate the influence of the material anisotropy. Therefore, the need for efficient numerical algorithms such as that discussed in the present paper is of utmost importance.

4.1.2 Uniaxial tension test

The second investigated example is the uniaxial tension test characterized by the stress tensors

$$\boldsymbol{P} = P_{11}\, \boldsymbol{e}_1 \otimes \boldsymbol{e}_1, \quad \boldsymbol{P} = P_{22}\, \boldsymbol{e}_2 \otimes \boldsymbol{e}_2, \quad \boldsymbol{P} = P_{33}\, \boldsymbol{e}_3 \otimes \boldsymbol{e}_3. \tag{97}$$

Again, the non-linear Neumann problem is solved by a Newton-type iteration.

In line with the previous subsection, monotonic tests are analyzed first. The computed results are summarized in Figs. 5 and 6. As for the shear test, the anisotropy of the elastic

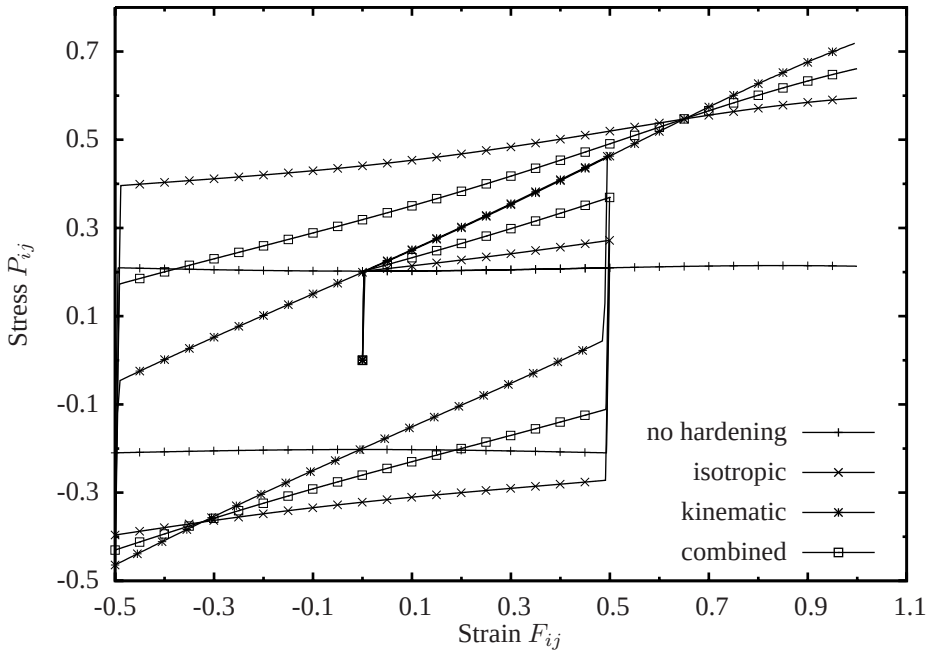

Figure 4: Hill-type model – cyclic shear test: stress-strain diagram associated with a fully anisotropic formulation (elastic and plastic) depending on the hardening model

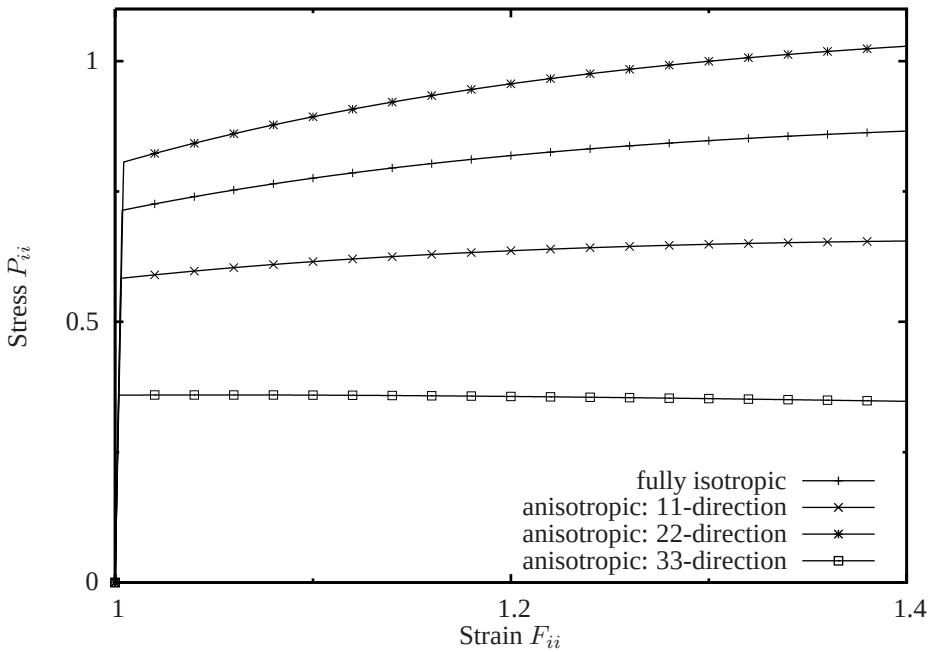

Figure 5: Hill-type model – monotonic uniaxial tension test: stress-strain diagram associated with isotropic hardening ($H_i = 1.0$, $H_k = 0.0$); results predicted by the fully anisotropic model (elastic and plastic) depending on the loading direction. For the sake of comparison, the response computed from the isotropic model (elastic and plastic) is shown as well.

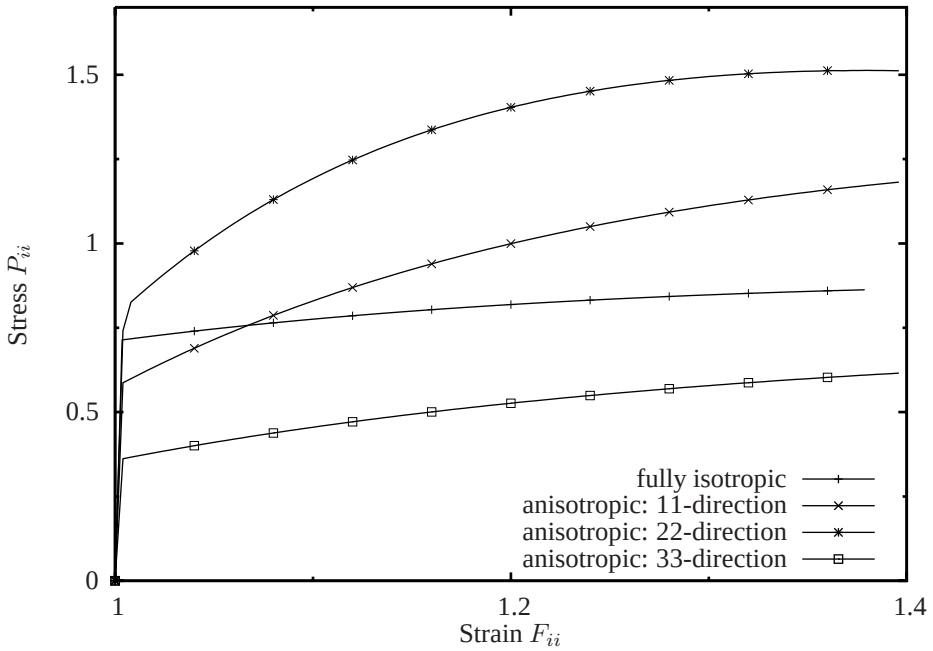

Figure 6: Hill-type model – monotonic uniaxial tension test: stress-strain diagram associated with kinematic hardening ($H_i = 0.0$, $H_k = 1.0$); results predicted by the fully anisotropic model (elastic and plastic) depending on the loading direction. For the sake of comparison, the response computed from the isotropic model (elastic and plastic) is shown as well.

domain, together with the loading direction depending hardening, is evident.

The numerically computed response corresponding to cyclic loading is shown in Figs. 7 and 8. In analogy to the simple shear test, all hardening models lead to identical results during the first loading stage, if a fully isotropic model is considered. By contrast, according to Fig. 8, orthotropy induces an additional coupling through which the influence of hardening becomes highly-nonlinear and complex.

It is noteworthy that the proposed constitutive update improves significantly the robustness as well as the performance compared to conventional update schemes. For instance, the computation of initial values for a Newton-iteration is far from being straightforward. Such problems do not occur within the advocated method. Furthermore, even if the considered mechanical model is highly non-linear or non-smooth reliable and powerful optimization methods are available, cf. [47, 48].

4.2 A modified Barlat-type model

Next, a constitutive model proposed by Cazacu & Barlat [34] is considered. It is based on a yield function of the type

$$\phi(\boldsymbol{\Sigma}) = (J_2^\circ)^{\frac{3}{2}} - J_3^\circ - (\tau_0^{\mathrm{eq}})^3 \,, \tag{98}$$

with

$$\begin{aligned} J_2^\circ = \; & \frac{a_1}{6}\,(\Sigma_{11}-\Sigma_{22})^2 + \frac{a_2}{6}\,(\Sigma_{22}-\Sigma_{33})^2 + \frac{a_3}{6}\,(\Sigma_{33}-\Sigma_{11})^2 \\ & + a_4\,\Sigma_{12}^2 + a_5\,\Sigma_{13}^2 + a_6\,\Sigma_{23}^2 \end{aligned} \tag{99}$$

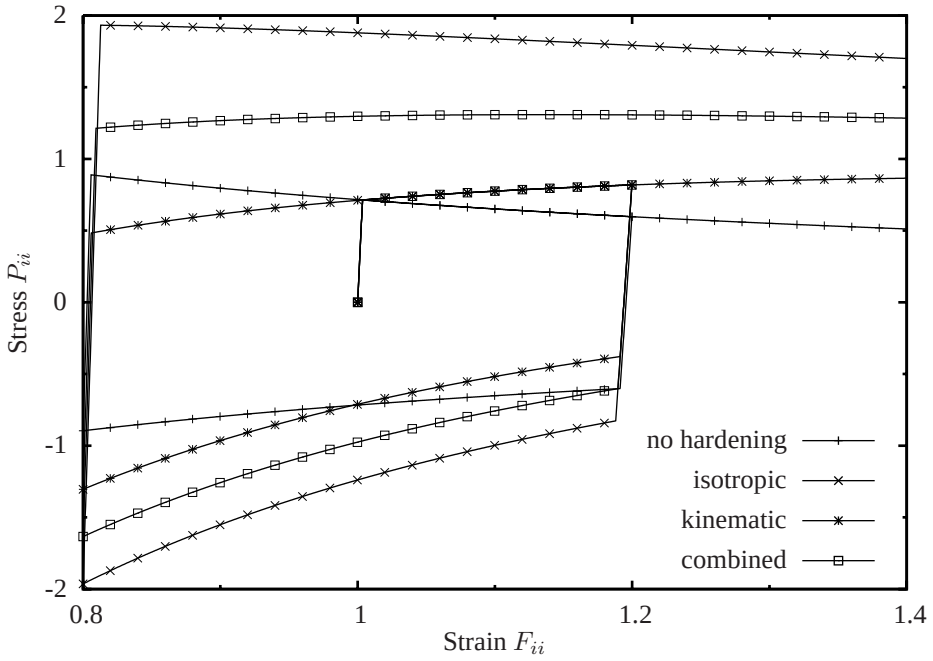

Figure 7: Hill-type model – cyclic uniaxial tension test: stress-strain diagram associated with a fully isotropic formulation (elastic and plastic) depending on the hardening model

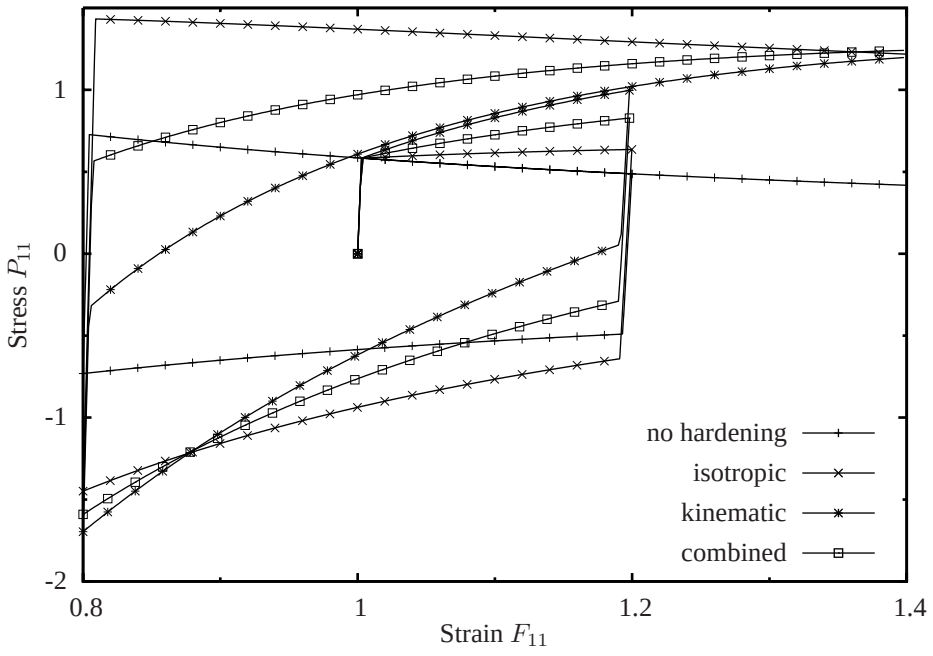

Figure 8: Hill-type model – cyclic uniaxial tension test: stress-strain diagram associated with a fully anisotropic formulation (elastic and plastic) depending on the hardening model

and

$$
\begin{aligned}
J_3^\circ = \;& \frac{1}{27}\;(b_1+b_2)\;\Sigma_{11}^3 + \frac{1}{27}\;(b_3+b_4)\;\Sigma_{22}^3 + \frac{1}{27}\;[2\,(b_1+b_4)-(b_2+b_3)]\;\Sigma_{33}^3 \\
& -\frac{1}{9}\;(b_1\,\Sigma_{22}+b_2\,\Sigma_{33})\;\Sigma_{11}^2 - \frac{1}{9}\;(b_3\,\Sigma_{33}+b_4\,\Sigma_{11})\;\Sigma_{22}^2 \\
& -\frac{1}{9}\;[(b_1-b_2+b_4)\;\Sigma_{11}+(b_1-b_3+b_4)\;\Sigma_{22}]\;\Sigma_{33}^2 + \frac{2}{9}\;(b_1+b_4)\;\Sigma_{11}\,\Sigma_{22}\,\Sigma_{33} \\
& +2\,b_{11}\,\Sigma_{12}\,\Sigma_{13}\,\Sigma_{23} - \frac{1}{3}\,\Sigma_{13}^2\;[2\,b_9\,\Sigma_{22}-b_8\,\Sigma_{33}-(2\,b_9-b_8)\;\Sigma_{11}] \\
& -\frac{1}{3}\,\Sigma_{12}^2\;[2\,b_{10}\,\Sigma_{33}-b_5\,\Sigma_{22}-(2\,b_{10}-b_5)\;\Sigma_{11}] \\
& -\frac{1}{3}\,\Sigma_{23}^2\;[(b_6+b_7)\;\Sigma_{11}-b_6\,\Sigma_{22}-b_7\,\Sigma_{33}]
\end{aligned}
\tag{100}
$$

Here, a_i and b_i are material parameters defining the anisotropy of the respective material and $\tau_0^{\rm eq}$ denotes the shear strength (In the original work [34], there is a typing error.). Following Remark 2, Eq. (98) being positively homogeneous of degree three is re-written into the positively homogeneous of degree one counterpart

$$
\phi(\boldsymbol{\Sigma},\alpha_{\rm i}) = \Big[(J_2^\circ)^{\frac{3}{2}} - (J_3^\circ)\Big]^{\frac{1}{3}} - \tau_0^{\rm eq} - Q_i(\alpha_{\rm i}) \tag{101}
$$

where $Q_{\rm i} := -\partial\Psi^{\rm p}/\partial\alpha_{\rm i}$ is associated with isotropic hardening. In contrast to the previous subsection, it is assumed that this internal variable saturates and converges to $Q_{\rm i}^\infty$. More precisely,

$$
Q_{\rm i}^{\rm eq}(\alpha_{\rm i}) = Q_{\rm i}^\infty\;\left(1-\exp\left[\alpha_{\rm i}/\alpha_{\rm u}\right]\right), \tag{102}
$$

with $\alpha_{\rm u}$ representing an additional material parameter.

The model is completed by the elastic response. Here, a stored energy functional based on a deviatoric/volumetric split is adopted, i.e.,

$$
\Psi^{\rm e} = \frac{1}{2}\,\mu\;\left(\mathrm{tr}\left[\boldsymbol{C}_{\rm dev}^{\rm e}\right]-3\right) + \frac{1}{4}\,K\;\left(J^{\rm e}-1\right)^2 \tag{103}
$$

with

$$
\boldsymbol{F}_{\rm dev}^{\rm e} := (J^{\rm e})^{-1/3}\;\boldsymbol{F}^{\rm e}, \quad \boldsymbol{C}_{\rm dev}^{\rm e} := (\boldsymbol{F}_{\rm dev}^{\rm e})^T\cdot\boldsymbol{F}_{\rm dev}^{\rm e} = (J^{\rm e})^{-2/3}\,\boldsymbol{C}^{\rm e}. \tag{104}
$$

The material parameters used for the numerical analysis correspond to sheets of Mg and are summarized in Tab. 4.

a_1	a_2	a_3	b_1	b_2	b_3	b_4
3.01742	4.63451	0.979594	-3.08191	2.77759	-2.30817	1.89439

E [MPa]	ν [-]	$\tau_0^{\rm eq}$ [MPa]	$Q_{\rm i}^\infty$ [MPa]	$\alpha_{\rm u}$ [-]
45000	0.33	48.5757	80.0	0.1

Table 4: Barlat-type model: material parameters chosen according to [52] (only the non-zero parameters are shown).

Following the previous subsection and in line with the experiments reported in [52], the material response is investigated by a uniaxial tensile test. Since Mg shows a pronounced

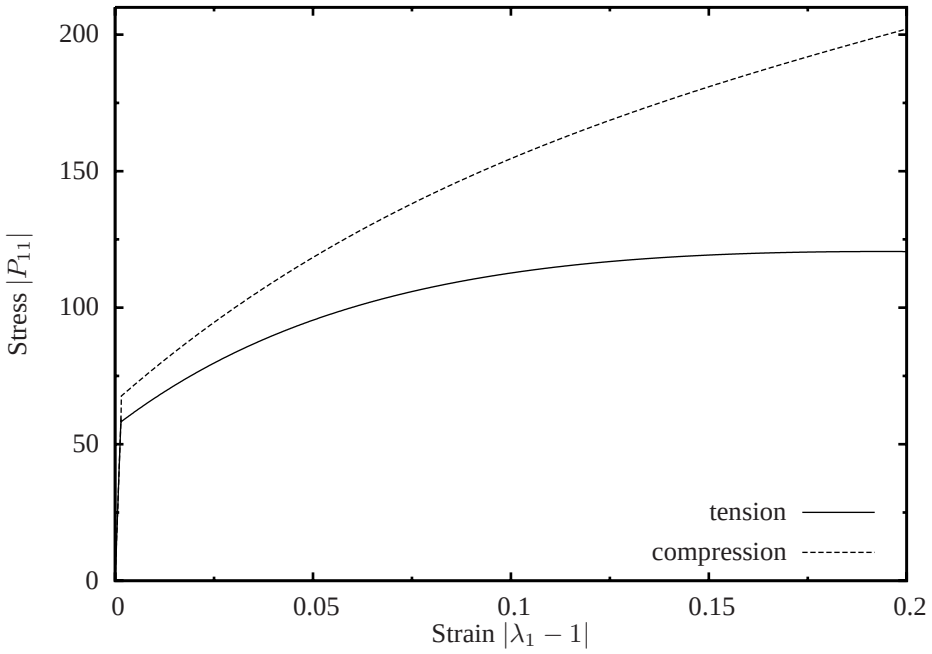

Figure 9: Barlat-type model: stress-strain-diagram predicted by the variational constitutive update for simple tension and simple compression.

tension/compression asymmetry, both loading cases are analyzed. The predicted mechanical responses are shown in Fig. 9. Although the model is highly anisotropic, even more pronounced than the Hill-type model, the variational constitutive update works very robustly and efficiently. Convergence problems did not occur. The computed mechanical response is in good agreement with the experiments reported in [52].

4.3 A strip with a hole

In contrast to the previous subsections, a mechanical problem characterized by a non-homogeneous stress state is numerically analyzed here. More precisely, a strip with a circular hole is considered, see Fig. 10. This example represents a standard benchmark being frequently applied to investigate the robustness and performance of plasticity models, cf. [2, 53]. For the purpose of comparison, the material model is chosen identically to that in [2, 53]. Consequently, a classical von Mises yield function is employed (see Subsection 4.1, Eq. (95) with $\mathbb{D} = \mathbb{I}$), while the elastic response is approximated by a Neo-Hooke-type model defined by the respective Helmholtz energy

$$\Psi^{\mathrm{e}}(\boldsymbol{F}^{\mathrm{e}}) = \frac{1}{2}\,\lambda\,\ln^2 \det(\boldsymbol{F}^{\mathrm{e}}) - \mu\,\ln\det(\boldsymbol{F}^{\mathrm{e}}) + \frac{1}{2}\,\mu\,(\boldsymbol{F}^{\mathrm{e}} : \boldsymbol{F}^{\mathrm{e}} - 3)\,. \tag{105}$$

Here, λ and μ are the Lamé constants depending on E and ν. Linear hardening is taken into account by using a quadratic stored energy functional Ψ^{p}. Two different models are analyzed. While the first of those is based on purely isotropic hardening ($H_{\mathrm{i}} = H^{\mathrm{eq}}$), the second shows a combined isotropic/kinematic hardening behavior ($H_{\mathrm{i}} = H_{\mathrm{k}} = 0.5\,H^{\mathrm{eq}}$).

For investigating the mechanical response predicted by the two different models, the distribution of the internal variable α_{i} and resulting load-displacement-diagrams are given in Fig. 11 and Fig. 12. According to these figures, both models (isotropic hardening and isotropic/kinematic hardening) lead to almost identical results. This is in line with the numerical analyses reported

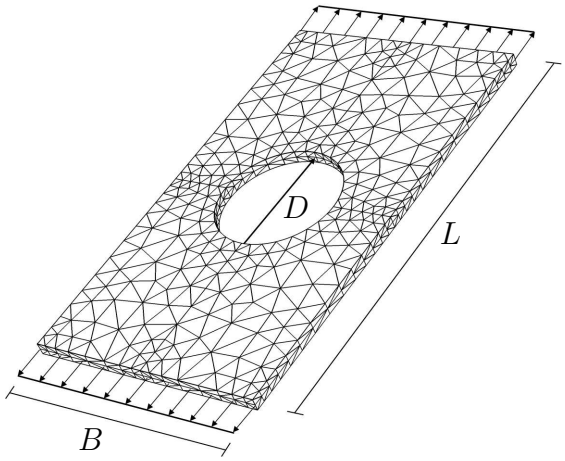

Geometry [cm]:		
L	36	
B	20	
D	10	
t	1.0	
Material parameters:		
E	70	kN/cm^2
ν	0.2	
$Q_0^{\rm eq}$	$\sqrt{2/3}$ 0.242	kN/cm^2
$H^{\rm eq}$	$\sqrt{2/3}$ 0.2	kN/cm^2

Figure 10: Strip with a circular hole: geometry, boundary conditions, finite element discretization (10-node purely displacement-driven tetrahedron elements) and material parameters. t denotes the thickness and $H^{\rm eq} := H_{\rm i} + H_{\rm k}$ represents an equivalent hardening parameter depending on the isotropic contribution $H_{\rm i}$ and the kinematic contribution$H_{\rm k}$.

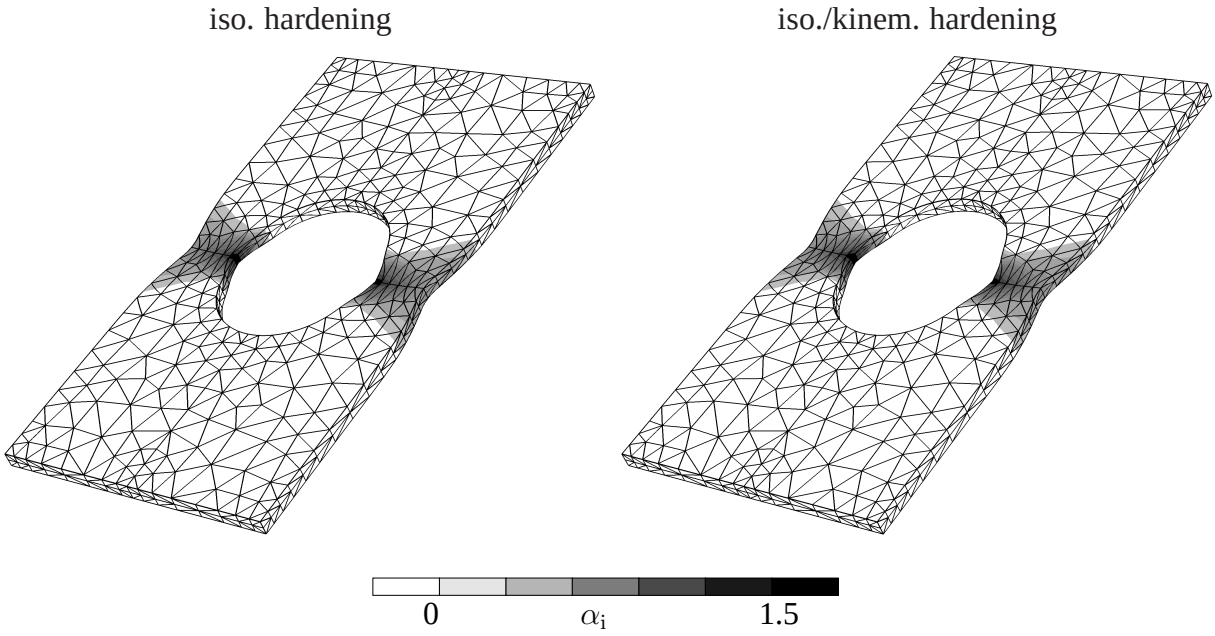

Figure 11: Strip with a circular hole: distribution of the isotropic hardening variable $\alpha_{\rm i}$ for a displacement amplitude of $u = 1.2$ cm (see Fig. 12). Left hand side: results predicted by isotropic hardening; Right hand side: results associated with the coupled isotropic/kinematic hardening model ($H_{\rm i} = H_{\rm k} = 0.5\ H^{\rm eq}$).

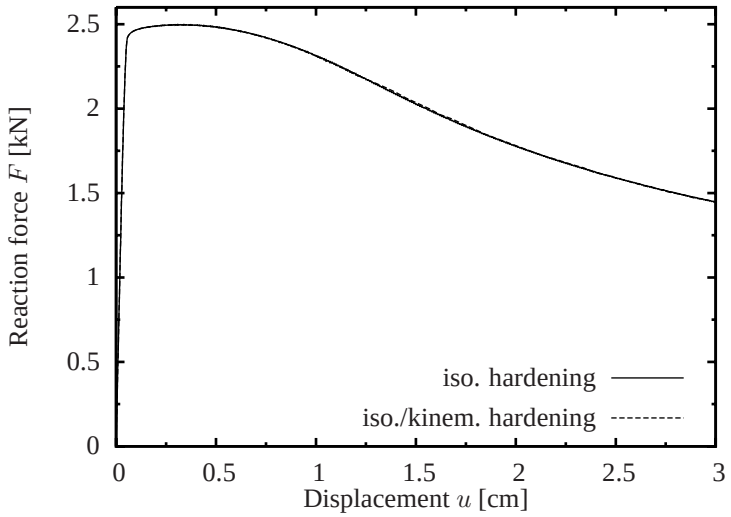

Figure 12: Strip with a circular hole: load-displacement diagram predicted by the isotropic and the combined isotropic/kinematic model.

in [54].

5 Conclusions

An enhanced constitutive update for so-called standard dissipative solids has been proposed. In contrast to conventional update schemes such as the by now classical return-mapping algorithm, the new method is fully variational. More precisely, and in line with the previous works [19, 22], the unknown history variables, together with the deformation mapping, follow jointly from minimizing an incrementally defined (energy) potential. Besides the associated mathematical and physical elegance, this method has some practical advantages. For instance, it allows to employ classical optimization methods for computing the solution of the aforementioned minimization problem. Unlike the prototype models advocated in [22–28], the proposed method covers a broad range of different constitutive models including anisotropic elasticity, anisotropic yield functions and isotropic as well as kinematic hardening. As relatively complex prototypes, an orthotropic Hill-type model including combined isotropic-kinematic hardening and an orthotropic modified Barlat-type model have been implemented. It has been shown that although the investigated prototypes represent highly non-linear, coupled and anisotropic problems, the advocated variational constitutive update works very robustly and efficiently.

References

[1] J.C. Simo. Numerical analysis of classical plasticity. In P.G. Ciarlet and J.J. Lions, editors, *Handbook for numerical analysis*, volume IV. Elsevier, Amsterdam, 1998.

[2] J.C. Simo and T.J.R. Hughes. *Computational inelasticity*. Springer, New York, 1998.

[3] A.L. Eterovic and K.-J. Bathe. A hyperelastic-based large strain elasto-plastic constitutive formulation with combined isotropic-kinematic hardening using the logarithmic stress and

strain measures. *International Journal for Numerical Methods in Engineering*, 30:1099–1114, 1990.

[4] J.C. Simo. Algorithms for static and dynamic multiplicative plasticity that preserve the classical return mapping schemes of the infinitesimal theory. *Computational Mechanics*, 99:61–112, 1992.

[5] A. Cuitiño and M. Ortiz. A material-independent method for extending stress update algorithms from small-strain plasticity to finite plasticity with multiplicative kinematics. *International Journal for Numerical Methods in Engineering*, 30:1099–1114, 1992.

[6] W. Dettmer and S. Reese. On the theoretical and numerical modelling of Armstrong-Frederick kinematic hardening in the finite strain regime. *Computer Methods in Applied Mechanics and Engineering*, 193:87–116, 2004.

[7] F. Amero. Energy-dissipative momentum-conserving time-stepping algorithms for finite strain multiplicative plasticity. *Computer Methods in Applied Mechanics and Engineering*, 195:4862–4889, 2006.

[8] S.N. Kuchnicki, A.M. Cuitiño, and R.A. Radovitzky. Efficient and robust constitutive integrators for single-crystal plasticity modeling. *International Journal of Plasticity*, 22:1988–2011, 2006.

[9] R.P.R. Cardoso and J.Y. Yoon. Stress integration method for a nonlinear kinematic/isotropic hardening model and its characterization based on polycrystal plasticity. *International Journal of Plasticity*, 2008. in press.

[10] S. Hartmann and W. Bier. High-order time integration applied to metal powder plasticity. *International Journal of Plasticity*, 24:17–54, 2008.

[11] M. Itskov. On the application of the additive decomposition of generalized strain measures in large strain plasticity. *Mechanics Research Communications*, 31:507–517, 2004.

[12] H. Xiao, O.T. Bruhns, and A. Meyers. Elastoplasticity beyond small deformations. *Acta Mechanica*, 182:31–111, 2006.

[13] R.J. Asaro. Micromechanics of crystals and polycrystals. *Advances in Applied Mechanics*, 23, 1983.

[14] M.L. Wilkins. Calculation of elasto-plastic flow. In B. Adler and et. al., editors, *Methods of computational physics*, volume 3. Academic Press, New York, 1964.

[15] E.A. de Souza Neto, D. Perić, and D.R.J. Owen. *Computational Methods for Plasticity: Theory and Applications*. Wiley & Sons, 2008.

[16] R. Hill. *The mathematical theory of plasticity*. Oxford University Press, Oxford, U.K., 1950.

[17] C. Comi, A. Corigliano, and G. Maier. Extremum properties of finite-step solutions in elastoplasticity with nonlinear hardening. *International Journal for Solids and Structures*, 29:965–981, 1991.

[18] C. Comi and U. Perego. A unified approach for variationally consistent finite elements in elastoplasticity. *Computer Methods in Applied Mechanics and Engineering*, 121:323–344, 1995.

[19] M. Ortiz and L. Stainier. The variational formulation of viscoplastic constitutive updates. *Computer Methods in Applied Mechanics and Engineering*, 171:419–444, 1999.

[20] R. Radovitzky and M. Ortiz. Error estimation and adaptive meshing in strongly nonlinear dynamic problems. *Computer Methods in Applied Mechanics and Engineering*, 172:203–240, 1999.

[21] M. Ortiz and E.A. Repetto. Nonconvex energy minimisation and dislocation in ductile single crystals. *J. Mech. Phys. Solids*, 47:397–462, 1999.

[22] C. Carstensen, K. Hackl, and A. Mielke. Non-convex potentials and microstructures in finite-strain plasticity. *Proc. R. Soc. Lond. A*, 458:299–317, 2002.

[23] M. Ortiz and A. Pandolfi. A variational Cam-clay theory of plasticity. *Computer Methods in Applied Mechanics and Engineering*, 193:2645–2666, 2004.

[24] Q. Yang, L. Stainier, and M. Ortiz. A variational formulation of the coupled thermo-mechanical boundary-value problem for general dissipative solids. *Journal of the Mechanics and Physics of Solids*, 33:2863–2885, 2005.

[25] E. Fancello, J.-P. Ponthot, and L. Stainier. A variational formulation of constitutive models and updates in non-linear finite viscoelasticity. *International Journal for Numerical Methods in Engineering*, 2005. in press.

[26] K. Weinberg, A. Mota, and M. Ortiz. A variational constitutive model for porous metal plasticity. *Computational Mechanics*, 37:142–152, 2006.

[27] T. El Sayed, A. Mota, F. Fraternali, and M. Ortiz. A variational constitutive model for soft biological tissue. *Journal of Biomechanics*, 41:1458–1466, 2008.

[28] E. Fancello, J.M. Vassoler, and L. Stainier. A variational constitutive update algorithm for a set of isotropic hyperelastic-viscoplastic material models. *Computer Methods in Applied Mechanics and Engineering*, 197:4132–4148, 2008.

[29] C. Miehe. Strain-driven homogenization of inelastic microstructures and composites based on an incremental variational formulation. *International Journal for Numerical Methods in Engineering*, 55:1285–1322, 2002.

[30] J.M. Ball. Convexity conditions and existence theorems in nonlinear elasticity. *Arch. Rat. Mech. Anal.*, 63:337–403, 1978.

[31] P. Thoutireddy and M. Ortiz. A variational r-adaption and shape-optimization method for finite-deformation elasticity. *International Journal for Numerical Methods in Engineering*, 61:1–21, 2004.

[32] J. Mosler and M. Ortiz. On the numerical implementation of variational arbitrary Lagrangian-Eulerian (VALE) formulations. *International Journal for Numerical Methods in Engineering*, 67:1272–1289, 2006.

[33] J. Mosler. *On the numerical modeling of localized material failure at finite strains by means of variational mesh adaption and cohesive elements*. Habilitation, Ruhr University Bochum, Germany, 2007.

[34] F. Cazacu, O.and Barlat. A criterion for description of anisotropy and yield differential effects in pressure-insensitive metals. *International Journal of Plasticity*, 20:2027–2045, 2004.

[35] E.H. Lee. Elastic-plastic deformation at finite strains. *Journal of Applied Mechanics*, 36:1–6, 1969.

[36] B.D. Coleman and M.E. Gurtin. Thermodynamics with internal state variables. *J. Chem. Phys*, 47:597–613, 1967.

[37] P.M. Naghdi. A critical review of the state of finite plasticity. *Zeitschrift für Angewandte Mathematik und Physik*, 315-394:41, 1990.

[38] S. Nemat-Nasser. *Plasticity : A Treatise on Finite Deformation of Heterogeneous Inelastic Materials*. Cambridge University Press, 2004.

[39] J. Lubliner. *Plasticity theory*. Maxwell Macmillan International Edition, 1997.

[40] C. Miehe. *Kanonische Modelle multiplikativer Elasto-Plastizität. Thermodynamische Formulierung und numerische Implementierung*. Habilitation, Forschungs- und Seminarbericht aus dem Bereich der Mechanik der Universität Hannover, Nr. F 93/1, 1993.

[41] J. Lubliner. On the thermodynamic foundations of non-linear solid mechanics. *International Journal of Non-Linear Mechanics*, 7:237–254, 1972.

[42] J. Mandel. *Plasticité Classique et Viscoplasticité*. Cours and Lectures au CISM No. 97. International Center for Mechanical Sciences, Springer-Verlag, New York, 1972.

[43] A.M. Maugin. *The thermodynamics of Plasticity and Fracture*. Cambridge University Press, 1992.

[44] O.T. Bruhns, H. Xiao, and A. Meyers. Some basic issues in traditional Eulerian formulations of finite elastoplasticity. *International Journal of Plasticity*, 19:2007–2026, 2003.

[45] J. Lemaitre and J.-L. Chaboche. *Mechanics of Solid Materials*. Cambridge University Press, 1994.

[46] H. Xiao. Private communication. 2007.

[47] C. Geiger and C. Kanzow. *Theorie und Numerik restringierter Optimierungsaufgaben*. Springer, 2002.

[48] C. Geiger and C. Kanzow. *Numerische Verfahren zur Lösung unrestringierter Optimierungsaufgaben*. Springer, 1999.

[49] M. Ortiz, R.A. Radovitzky, and E.A. Repetto. The computation of the exponential and logarithmic mappings and their first and second linearizations. *International Journal for Numerical Methods in Engineering*, 52(12):1431–1441, 2001.

[50] M. Itskov. Computation of the exponential and other isotropic tensor functions and their derivatives. *Computer Methods in Applied Mechanics and Engineering*, 192(35-36):3985–3999, 2003.

[51] J. Löblein. *Ein Modell zur Beschreibung finiter anisotroper elasto-plastischer Deformationen unter Berücksichtigung diskreter Rissausbreitung*. PhD thesis, Universität Duisburg-Essen, 2004.

[52] M. Nebebe, J. Bohlen, D. Steglich, and D. Letzig. Mechanical characterization of Mg alloys and model parameter identification for sheet forming simulations. In *Esaform*, 2009. in press.

[53] P. Fuschi, D. Perić, and D.R.J. Owen. Studies on generalized midpoint integration in rate-independent plasticity with reference to plane stress J_2-flow theory. *Computers & Structures*, 43:1117–1133, 1992.

[54] O. Kintzel. *Modellierung elasto-plastischen Materialverhaltens und duktiler Porenscgädigung metallischer Werkstoffe bei großen Deformation*. PhD thesis, Ruhr-University-Bochum, 2007.